Quantitative dating of Pleistocene deposits of the Kyrenia Range, northern Cyprus: implications for timings, rates of uplift and driving mechanisms

JGS
Journal of the Geological Society

Research article

Published Online First

doi:10.1144/jgs2015-130

Quantitative dating of Pleistocene deposits of the Kyrenia Range, northern Cyprus: implications for timing, rates of uplift and driving mechanisms

Romesh N. Palamakumbura[1]*, Alastair H. F. Robertson[1], Tim C. Kinnaird[2], Peter van Calsteren[3], Dick Kroon[1] & Jenny A. Tait[1]

[1] School of GeoSciences, Grant Institute, University of Edinburgh, James Hutton Road, Edinburgh EH9 3FE, UK
[2] SUERC, Rankine Avenue, Scottish Enterprise Technology Park, East Kilbride G75 0QF, UK
[3] EEE, The Open University, Walton Hall, Milton Keynes MK7 6AA, UK
* Correspondence: rpalamakumbura@gmail.com

Abstract: The Kyrenia Range underwent tectonically driven uplift during the Pliocene to Pleistocene in response to the interaction of various tectonic processes. To understand the tectonic processes driving the uplift and how this is related to uplift of other areas of the Eastern Mediterranean, uranium-series disequilibrium and optically stimulated luminescence dating were applied to marine and non-marine terrace deposits exposed on the northern flank of the range. Palaeomagnetism and strontium isotope dating were used in conjunction to date the final stages of the marine environment adjacent to the Kyrenia Range prior to major surface uplift. Uplift rates range from >1.2 mm a^{-1}, inferred during the Early Pleistocene, to <0.2 mm a^{-1} during the Late Pleistocene. The new data show that the Kyrenia Range was uplifted contemporaneously with the Troodos Massif in southern Cyprus. The uplift of the Kyrenia Range appears to have been significantly faster than that affecting other comparable regions in the easternmost Mediterranean during the Pleistocene (e.g. Lebanon coast; southern Anatolian plateau). The driving mechanism for the uplift of both the Kyrenia Range and the Troodos Massif is inferred to be the collision of the Eratosthenes Seamount with the Cyprus trench to the south of Cyprus.

Supplementary material: Details of the methods used are available at https://doi.org/10.6084/m9.figshare.c.3260977.

Received 28 October 2015; **revised** 20 February 2016; **accepted** 22 March 2016

The main aim of this paper is to present and discuss the results of quantitative dating of Pliocene and Pleistocene deposits associated with the Kyrenia Range with a view to understanding the timing, rates and processes driving its surface uplift. Similar studies have been carried out on other areas, such as the Miocene to Recent uplift of the Andes (Gregory-Wodzicki 2000) and the Late Cenozoic uplift of southeastern Tibet (Clark *et al.* 2005). A key current objective of geological and geomorphological research is the identification of the crustal processes involved in surface uplift. The Eastern Mediterranean region is very well suited to this approach because it is an active tectonic area that is becoming increasingly well understood based on a combination of both land and marine geophysical and geological studies. The easternmost Mediterranean region (Fig. 1) is a convergence zone involving subduction, strike-slip (including transpression and transtension) and collision at different scales, together with deep-seated processes such as crustal delamination, slab break-off and slab tearing (Faccenna *et al.* 2006; Berk Biryol *et al.* 2011; Schildgen *et al.* 2012; Bartol & Govers 2014). The interaction of such deep-seated tectonic processes drives surface uplift in various parts of the easternmost Mediterranean and the adjacent region. For example, major surface uplift occurred during the Plio-Pleistocene in the Peloponnese and elsewhere in Greece (Roberts *et al.* 2009; Turner *et al.* 2010) and in the Taurus Mountains of southern Turkey (Schildgen *et al.* 2012).

Previous work has documented the uplift of the Troodos Massif in the south of Cyprus, which climaxed during the Pleistocene (Gass 1960; De Vaumas 1961; Poole *et al.* 1990; Poole & Robertson 1991, 2000; Robertson & Xenophontos 1993; Kinnaird *et al.* 2011; Kinnaird & Robertson 2013; Main *et al.* 2016). The Troodos Massif is a Late Cretaceous ophiolite (subaerially exposed oceanic crust), overlain by Late Cretaceous to Recent deep-marine to shallow-marine and non-marine sediments. The likely cause of the uplift of the Troodos Massif was the collision of the Eratosthenes Seamount, a large crustal edifice, with the Cyprus active margin, related to a northward-dipping subduction zone. The uplift was possibly localized and accentuated by the effects of serpentinization of the oceanic mantle wedge by fluids derived from the downgoing slab (Robertson 1990, 1998*b*, 2000; Kempler 1998).

Sandwiched between southern Turkey and the Troodos Massif is the Kyrenia Range, an approximately east–west-trending narrow, arcuate mountain range in the northern part of Cyprus. The western end of the Kyrenia Range reaches *c.* 1000 m above modern sea level (AMSL); the range decreases in height eastwards overall and then passes into a submerged ridge that links with the Misis Mountains of southern Turkey (Fig. 1). Previous studies have suggested that the Kyrenia Range is of relatively recent origin (Ducloz 1972; Baroz 1979) but the detailed timing and processes involved remained elusive. New evidence for the uplift is presented here in relation to adjacent areas and alternative interpretations are discussed in their regional context.

Geological background

The regional geology of the area concerned may influence the nature of any uplift, including features such as the relative competency of lithologies and inherited structure.

In outline, the Kyrenia Range has a Late Palaeozoic to Recent geological history with four main stages of stratigraphical development. These encompass the deposits of the Trypa (Tripa), Lapithos (Lapta), Kythrea (Değirmenlik) and Mesaoria (Mesarya)

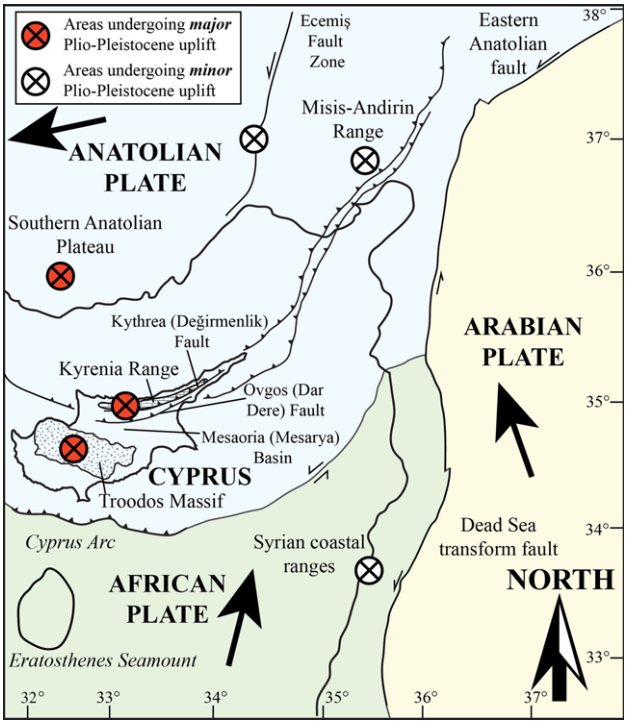

Fig. 1. Summary diagram of the regional tectonic setting of Cyprus during the Pliocene to Pleistocene, adapted from Kempler & Garfunkel (1994) with additional information from Barka & Reilinger (1997), McClusky *et al.* (2003), Jaffey & Robertson (2001), Calon *et al.* (2005*a*), Dilek & Sandvol (2009), Schattner (2010), McCay & Robertson (2012*b*) and Schildgen *et al.* (2012).

Groups (it should be noted that the nomenclature follows stratigraphic priority; Fig. 2). We use the traditional stratigraphic names, followed by recent Turkish equivalents. The Trypa (Tripa) Group is dominated by neritic metacarbonates of Triassic to Cretaceous age (Ducloz 1972; Baroz 1979; Robertson & Woodcock 1986). The Lapithos (Lapta) Group unconformably overlies the Trypa (Tripa) Group and comprises pelagic carbonates interbedded with subaqueous basic or silicic volcanic rocks and also sedimentary mélange (olistostromes), of overall Maastrichtian to Eocene age (Robertson *et al.* 2012). The unconformably overlying Kythrea (Değirmenlik) Group comprises Late Eocene to Late Miocene, mostly marine conglomerates, sandstones, marls and mudstones, culminating in Messinian evaporites (Weiler 1970; McCay 2010; McCay & Robertson 2012*a*; McCay *et al.* 2012; Taylforth *et al.* 2014). Unconformably above comes the Mesaoria (Mesarya) Group, represented by Pliocene shallow-marine to non-marine sediments (Ducloz 1972; Baroz 1979; McCay & Robertson 2012*a*; McCay *et al.* 2012). The Mesaoria (Mesarya) Group includes the Myrtou (Çamlıbel), Nicosia (Lefkoşa), Athalassa (Gürpınar) and Fanglomerate Formations (Baroz 1979). Of these, the Myrtou (Çamlıbel) Formation comprises interbedded marls and siltstones (Baroz 1979; Yetis *et al.* 1995; McCay *et al.* 2012), whereas the Nicosia (Lefkoşa) Formation is made up of interbedded marls and chalks (Baroz 1979; Yetis *et al.* 1995). Above this, the Athalassa (Gürpınar) Formation is predominantly shallow-marine carbonate grainstones (Baroz 1979; McCallum & Robertson 1995*a*; Harrison *et al.* 2004). Finally, the traditional Fanglomerate Formation is represented by a series of terrace deposits on both flanks of the Kyrenia Range (Ducloz 1964; Knup 1965; Baroz 1979).

The opposing flanks of the Kyrenia Range are characterized by terraced littoral-marine and non-marine sediments, up to a height of *c.* 180 m AMSL. These deposits were previously mapped and described as being Pleistocene (Ducloz 1972; Dreghorn 1978), although no absolute age data were available. Based on extensive new fieldwork (Palamakumbura 2015; Palamakumbura *et al.* 2016), five main terraces are now identified on the northern and the southern flanks of the range, defined as K0–K5 (Figs 2 and 3a). The K0 terrace is the highest and, by inference, the oldest terrace, whereas the K5 terrace is the lowest and youngest terrace. In terms of the previous stratigraphy the K0, K1, K2, K3, K4 and K5 terraces are equivalent to the Karka, Klepini (Arapköy), Trapeza (Beşparmak), Ayios Epikititos (Çatalköy), Kyrenia (Girne) and Koupia terraces, respectively (Ducloz 1972). The highest terrace, K0, is preserved at *c.* 800–600 m AMSL. The K0 terrace comprises non-marine megabreccia with no preserved marine facies. The K1 terrace is preserved on the distal parts of the K0 terrace at 600 m AMSL and comprises colluvial conglomerates. The K2, K3 and K4 terrace deposits, which include shallow-marine facies, are preserved at *c.* 180–140, 70–50 and 40–0 m AMSL, respectively. Finally, the K5 terrace is preserved along the northern coast at modern sea level. The age progression of the terraces has been inferred from outcrop field relations, including incision and facies geometry, and was also tested by the age dating presented here. The heights of each terrace are taken from the most northerly part of each terrace, closest to the coast, reflecting the basal and oldest part of each terrace system. The height above sea level of each terrace was established from a combination of the contoured base of the published geological maps of the central Kyrenia Range (Ducloz 1964; Knup 1965), handheld global positioning system (GPS) measurements and Google Earth. The estimated error in the heights is <5 m, whereas the variation in height between each of the terrace systems (other than the two youngest ones) is several tens of metres or more. Uncertainties in absolute height do not compromise our discussion of the processes of uplift v. sea-level change.

The structure of the Kyrenia Range and the adjacent Mesaoria (Mesarya) Basin has been documented based on regional mapping (Baroz 1979) from outcrop-scale observations and microstructural studies (McCay & Robertson 2012*a*; Robertson & Kinnaird 2016). The last of several major phases of deformation corresponds to an important phase of southward thrusting during Late Miocene–earliest Pliocene time in a left-lateral, transpressional stress regime (the earlier structural history is not considered here). Pleistocene compression or transpression is locally documented by faults that cut Pliocene sediments (McCay & Robertson 2012*b*). In addition, a small number of transverse fault planes within the Kyrenia Range are mantled by relatively immature scree talus, of inferred Pleistocene age (e.g. NNW–SSW-trending fault lineament near Beşparmak (Pentadactylos mountain) (Robertson & Kinnaird 2016)). There is also evidence of Pliocene–Pleistocene sinistral strike-slip movements along the Ovgos (Dar Dere) Fault to the south of the Kyrenia Range (Harrison *et al.* 2004).

Here, we combine field-based studies of the Pliocene and Pleistocene sediments with absolute age dating using several well-established techniques, each of which have pros and cons. Classical biostratigraphy (e.g. using macrofossils) is of limited use to date the Pliocene–Pleistocene sediments because most of the species present are relatively long ranging. All but possibly the very youngest sediments are expected to be beyond the age range of radiocarbon dating. Optically stimulated luminescence (OSL) is potentially useful, but only for sediments of <200 ka age (for quartz) and <500 ka age (for feldspar) (Rhodes 2011). Similarly, uranium-series disequilibria (U-series) dating is unlikely to be viable at >350 ka (Van Calsteren & Thomas 2006). U-series dating depends on analysing aragonitic coral, which although present is relatively rare. Other macrofossils including bivalves rarely provide reliable results (Van Calsteren & Thomas 2006). Magnetostratigraphy has obvious potential, following successful studies of similar deposits in the south of Cyprus (Kinnaird *et al.* 2011; Weber *et al.* 2011), but

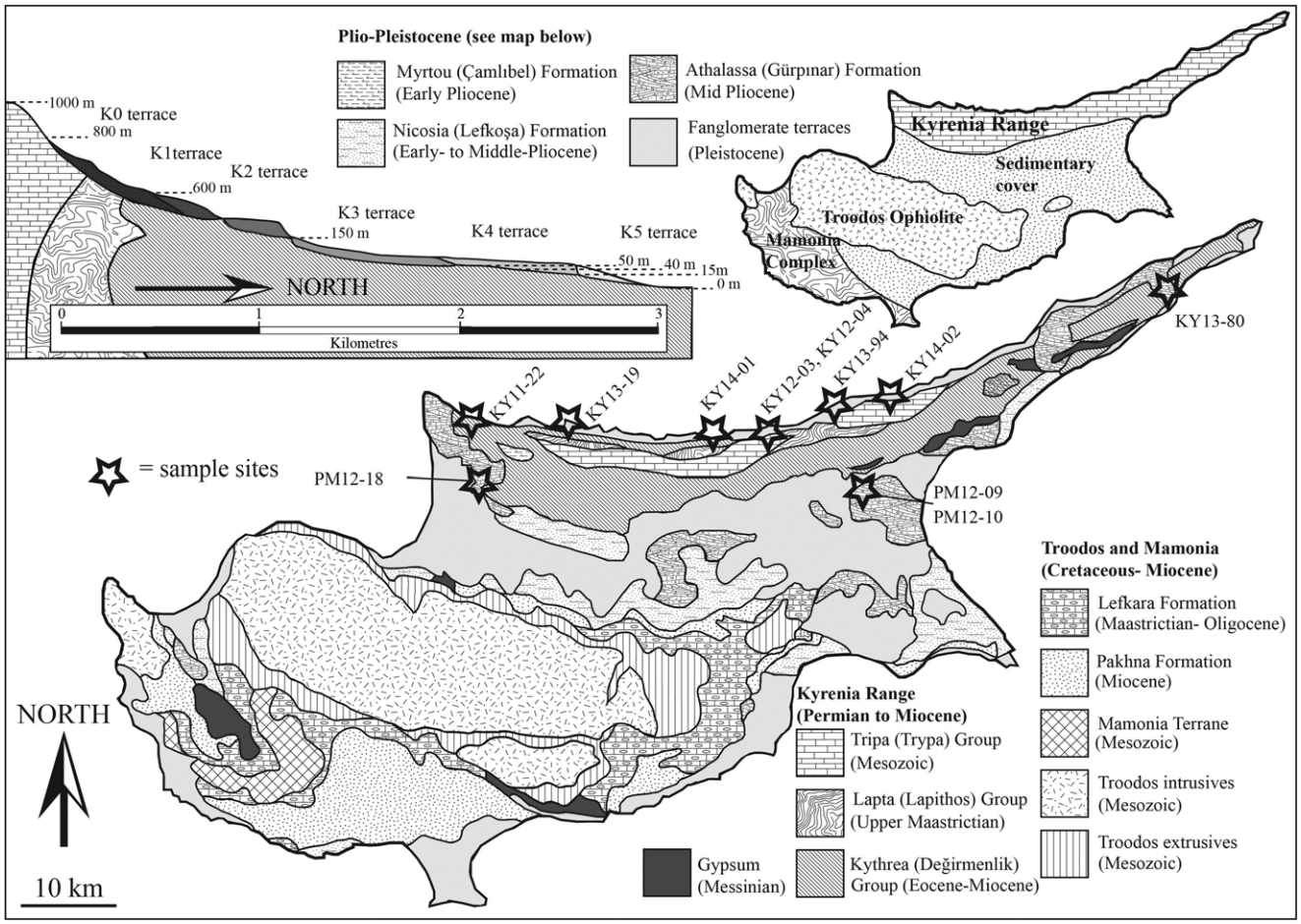

Fig. 2. Simplified geological map of Cyprus with emphasis on the distribution of Pliocene and Pleistocene deposits together with a simplified cross-section showing the heights above modern sea level of the K0–K5 terraces on the northern flank of the Kyrenia Range. The sample localities are indicated. Adapted from McCay & Robertson (2012*b*) and McCay *et al.* (2012).

is dependent on the sediments preserving measurable stable magnetic remanence that is indicative of magnetic polarity (Kodama 2012). Strontium isotopic analysis is also useful but only for the dating of suitable, well-preserved fossils from an open-marine setting (Beets & De Ruig 1992; Müller 1993). Exposure dating could also have potential, although detailed geomorphological analysis was outside the scope of this work.

In practice, some valid new data were obtained with each of the techniques used, although all of these are problematic in one way or another. The techniques used followed well-established methods. U-series and OSL dating proved suitable for dating of the younger marine terraces (K4 and K5) on the northern flank of the range. In addition, microfossil evidence, mostly from planktonic foraminifera, and palaeomagnetic data were effective for dating shallow-marine sediments that were deposited before major uplift of the range.

Uplift deposits and dating

U-series dating was carried out on well-preserved solitary corals (*Cladocora caespitosa*) (Fig. 3b and c). The corals were collected from the K4 terrace along the northern coast. The best-preserved coral samples came from two marine deposits, as summarized in Table 1. The first dated deposit is a marine conglomerate, which includes well-rounded and well-sorted clasts of locally derived 'basement' rocks (e.g. metacarbonate rocks, basalt, chert), ranging in size from 1 to 10 cm. Large amounts of biogenic material also occur within the conglomerate including oysters, pectens, gastropods, serpulid worms (as casts), molluscs (commonly bored) and solitary coral. The second dated deposit is a breccia of well-cemented marine bioclastic grainstone (Table 1). This is fine to medium grained and contains abundant reworked biogenic material including molluscs, serpulid worm casts, bored clasts and solitary coral. The observed marine grainstone is interbedded with a Gilbert-type deltaic deposit.

OSL dating was carried out on aeolian grainstones of the K5 terrace on the northern coast (Fig. 3d and e). The grainstones (Table 1) are medium grained and contain well-sorted and well-rounded grains. The coastal grainstones contain well-preserved trough cross-bedding, with 1–3 m thick foresets. Calcified palaeo-root traces are well preserved throughout the aeolian deposits. In a related study, the grainstone deposits have been profiled in the field using a portable OSL reader to assess their luminescence characteristics (Palamakumbura *et al.* 2016). This study showed that these sediments contain sufficient quartz and feldspar with sufficient luminescence signal to permit dating. The deposit is interpreted as representing a coastal aeolian dune environment (Palamakumbura 2015; Palamakumbura & Robertson 2016; Palamakumbura *et al.* 2016).

Uranium-series disequilibrium dating

Solitary corals are relatively rare in the littoral marine terrace deposits along the northern coast. Also, some of those collected were found, based on X-ray diffraction (XRD) analysis, to be partially recrystallized and so unsuitable for dating (Palamakumbura 2015). Following extensive fieldwork, five solitary coral samples were selected for dating from four sites within the K4 terrace along the northern coast (Fig. 2). The selected corals are preserved *in situ* without reworking and are, therefore, believed to represent the age of

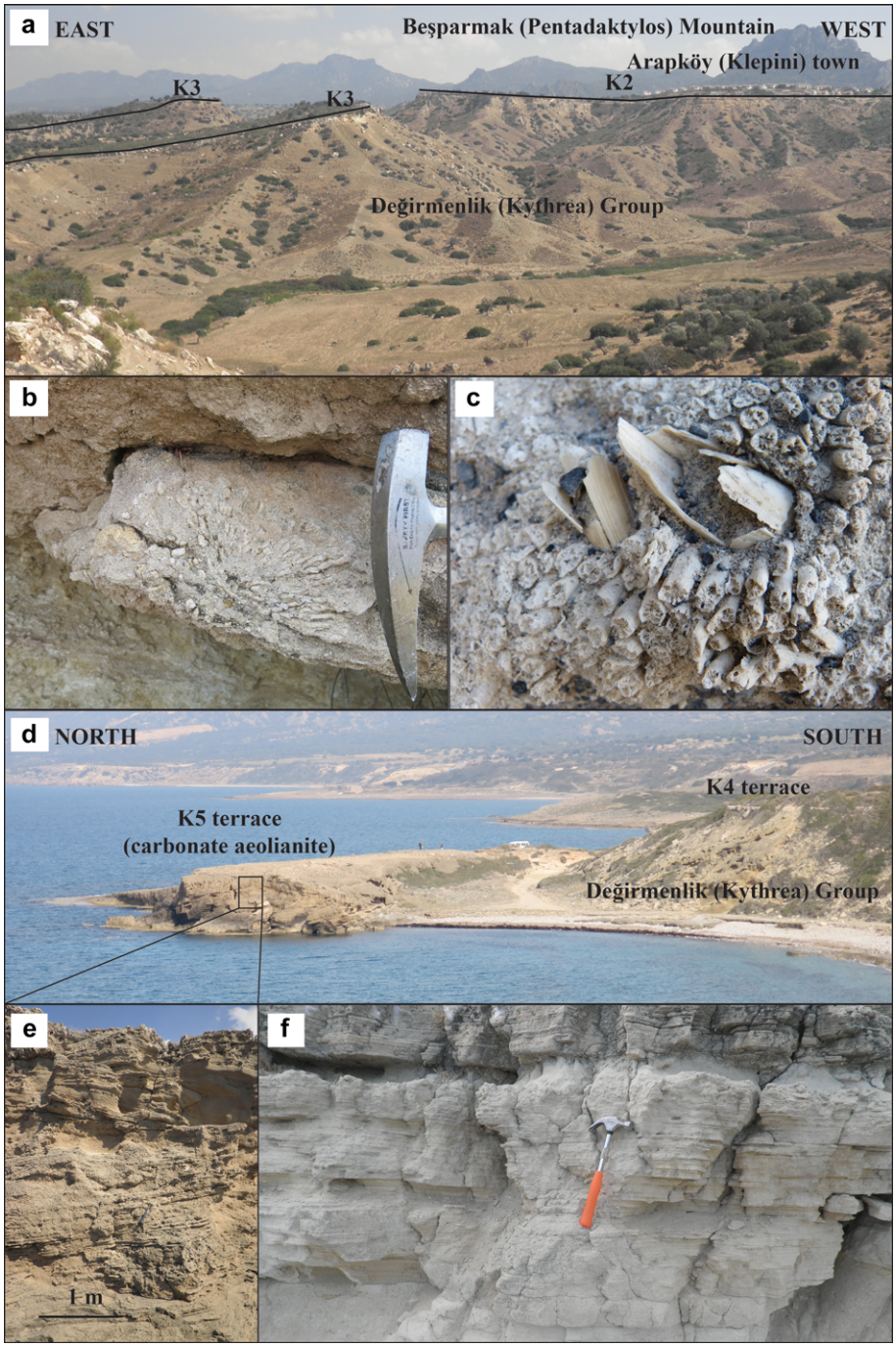

Fig. 3. Photographs of the terraces of northern Cyprus and the various dated deposits. (**a**) An overview of the K2 and K3 terraces within the central part of the Kyrenia Range; (**b**, **c**) *Cladocora* solitary coral preserved within the K4 terrace; (**d**, **e**) K5 terrace aeolianites along the northern coast; (**f**) planar-bedded grainstone of the Athalassa (Gürpınar) Formation.

the marine deposit in which they are preserved. The coral samples were cut into several subsamples, with the central septa being removed and the walls cleaned with a Dremel drill©. XRD analysis was carried out on the coral-wall samples. Only coral samples with over 97% aragonite were used for dating.

The facies of the deposits containing the corals is indicative of a major marine transgression event followed by a marine regression. In addition, relatively minor transgressive events are indicated by the presence of thin (tens of centimetres) layers of coral-bearing deposits within otherwise regressive sedimentary sequences, as discussed in detail elsewhere (Palamakumbura 2015; Palamakumbura & Robertson 2016; Palamakumbura *et al.* 2016).

The U-series dating was carried out at the Open University, Milton Keynes, using standard methods: further information has been given by Van Calsteren & Thomas (2012). Samples KY12-03, KY12-04 and KY11-22 have $^{230}Th/^{234}U$ ratios of <1 (Table 2). In contrast, samples KY13-19(b), -94(a) and -94(b) exhibit $^{230}Th/^{234}U$ ratios of *c.* 1, indicating either that the system has reached secular equilibrium or that thorium isotopic contamination has taken place. The ^{232}Th concentrations are low enough to suggest that thorium contamination is not a significant issue for any of the samples (Table 2). The samples KY13-19(b), -94(a) and -94(b) are, therefore, assumed to be in secular equilibrium. Table 2 shows the final calculated ages of the coral samples, as determined from the relationship between uranium and thorium isotopes (Ivanovich 1982). The five coral samples yielded ages ranging from 127 to >350 ka (Middle Pleistocene).

Optically stimulated luminescence

The luminescence dating analysis was carried out at the Scottish Universities Environmental Research Centre (SUERC) luminescence laboratories, East Kilbride. Conventional OSL quartz and also post-infra-red elevated temperature infra-red-stimulated

Table 1. *Summary of the sedimentology of the dated deposits along the northern flank of the Kyrenia Range and in the Mesoaria (Mesarya) Plain (see also Palamakumbura & Robertson 2016)*

Sample number	Analytical technique	Dated material	Deposit description	Interpretation
KY13-19, -94a, b	U-series	Coral (shoreface conglomerate) (Fig. 3b)	Corals preserved within clast-supported conglomerate with sub-angular clasts. Clasts range in size from 1 to 10 cm and comprise reworked grainstone and packstone, metacarbonate, chalk, chert and basalt. Biogenic material includes oysters, pectens, gastropods, serpulid worm casts and boring molluscs. The deposits comprised a medium-grained well-lithified carbonate sand matrix. The deposits are 30–50 cm thick and preserved at the base of marine terrace deposits, erosionally overlying basement.	The conglomerates are interpreted as tempestite (storm) deposits, proximal to the coast with reworked coral-rich material
KY12-03, -04	U-series	Coral (grainstone breccia interbedded with deltaic deposits) (Fig. 3c)	Conglomerate clasts ranging from 1 cm to nearly 2 m and composed of well-cemented fine-grained grainstone. Grainstone clasts are angular and only locally reworked. The grainstone contains well-preserved molluscs and serpulid worms tubes. Corals are well preserved *in situ*. The conglomerate is interbedded with a cross-bedded gravel deposit.	An offshore marine deltaic system (represented by the cross-bedded gravel)
KY11-22	U-series	Coral (shallow-marine conglomerate)	Corals are preserved within a conglomerate that is clast supported and comprises well-rounded siliciclastic and bioclastic material, including metacarbonate, mudstone, chert, diabase, serpentinite, pectens, oysters, gastropods, calcareous algae and serpulid worm tubes. The conglomerate comprises 0.5–1 m-thick parallel beds with well-developed normal grading and clasts ranging from 1 to 10 cm in size. Conglomerate beds are separated by 0.5–2 m thick marl beds.	Shallow-marine environment with episodic high-energy conglomerate input. Coral formed during marine highstands in relatively low-energy conditions and was locally reworked
KY14-01, -02	OSL	Aeolian grainstone (Fig. 3d and e)	Medium- to fine-grained grainstone with abundant calcified root traces throughout. Grains are composed of both siliciclastic and bioclastic material and are generally well rounded and well sorted. The deposits contain 1–3 m-thick trough cross-bedding, with variable palaeocurrent directions. The grainstone are well lithified with a micritic cement.	Onshore coastal dune fields
KY13-80	Strontium isotopes	Carbonate grainstone (Fig. 3f)	Fine-grained grainstone with 20–30 cm-thick parallel bedding. Grains are predominantly benthic foraminifera together with minor siliciclastic material. The deposits are well lithified with a micritic cement.	Low-energy open-marine basin
PM12-09, -10, -18	Palaeomagnetism			

luminescence (i.e. post-IR IRSL) potassium feldspar approaches were initially considered as potential methods for dating the aeolianite. The regional geology is dominated by calcareous rocks of Permian to Middle Miocene age, together with subordinate volcanogenic and siliceous rocks. This is challenging because locally derived sands are largely composed of low-radioactivity materials with little quartz or alkali feldspar. However, luminescence profiling, both during the fieldwork and subsequently in the laboratory revealed stratigraphically progressive OSL and IRSL signals (Palamakumbura *et al.* 2016), indicating the presence of material in the sediments with dating potential. Although the laboratory characterization indicated the presence of some quartz, its low yields and low luminescence sensitivity, and (on further investigation) the lack of thermal stability of the conventional OSL signals (i.e. the fast component) precluded application of quartz-based methods. Electron microscopy confirmed the presence of feldspars, which were separated and used instead of quartz for IRSL and elevated temperature post-IR IRSL single aliquot regeneration (SAR) dating (Buylaert *et al.* 2009; Thomsen *et al.* 2011; Kinnaird *et al.* 2015).

Dose-rate estimates from the carbonate sands were assessed using a combination of field gamma spectrometry, high-resolution gamma spectrometry (HRGS) and thick-source beta counting (TSBC), which were reconciled with each other and with the water contents and micro-dosimetry of the model. In addition to the two dating samples, a series of eight bulk gamma spectrometry samples were collected to permit retrospective analysis of the external gamma dose rates. The gamma dose rates were reconstructed from seven of these, giving wet gamma dose rates of between 0.4 and 0.7 mGy a^{-1}, which are comparable with the measured values recorded at the sampling positions (0.4–0.5 mGy a^{-1}). Counting times for both HRGS and TSBC measurements were extended by one order of magnitude, resulting in overall uncertainties of <4% for these low dose rates. Internal alpha dose rates were estimated on the basis of inductively coupled plasma mass spectrometry (ICP-MS) analysis

Table 2. *Uranium and thorium isotope results from Cladocora solitary corals of the K4 terrace*

Sample	Latitude, longitude	Height (m AMSL)	$^{234}U/^{238}U$	Error	$^{230}Th/^{234}U$	Error	^{232}Th (ppb)	Error	Age (ka)	Error (ka)
KY13-19b	35°21.627'N, 33°08.277'E	5	1.0186	0.0099	1.1192	0.0401	193.64	35.08	>350	–
KY13-94a	35°24.5209'N, 33°45.509'E	15	0.9986	0.0107	1.0610	0.0380	57.93	10.50	>350	–
KY13-94b	35°24.5209'N, 33°45.509'E	15	0.9952	0.0102	1.0703	0.0383	54.97	9.96	>350	–
KY12-03	35°20.870'N, 33°34.372'E	4	1.1052	0.0109	0.7069	0.0232	203.55	36.88	127	21.14
KY12-04	35°20.870'N, 33°34.372'E	4	1.0961	0.0093	0.7192	0.0236	248.66	45.05	131	22.55
KY11-22	35°21.458'N, 33°02.814'E	40	1.0946	0.0051	0.9163	0.0083	190.75	34.48	243	19.53

of comparable feldspars and make a minor contribution to the overall dose rates from this material.

Equivalent doses were determined from 16 aliquots of K-feldspar per sample using IRSL and elevated temperature post-IR IRSL SAR protocols. The material exhibited good IRSL sensitivity and produced acceptable SAR internal quality control performance. On the basis of these results, coupled with the IRSL SAR quality selection criteria and the expectations of the procedure, preference was given to the post-IR IRSL 225°C signals in equivalent dose determinations (Fig. 4). Radial plotting methods revealed some heterogeneity in the equivalent dose distributions of each sample, reflecting variable bleaching at the time of deposition and indicating that each sample enclosed mixed-age materials (Fig. 4c). The laboratory profiles provide some measure of control on this. The basal parts of each deposit show the greatest dispersion or spread in IRSL stored dose values, and, importantly, the lowest values in each profile. In contrast, the upper units are characterized by larger IRSL stored dose values with tighter distributions, reflecting faster deposition and poor to incomplete bleaching, or zeroing, of the luminescence signals. The mean ratios of sensitization-independent stored to prompt normalized signals after 10^6 s storage are 0.93 ± 0.06 and 1.08 ± 0.08, for IRSL and post-IR IRSL 225°C, respectively.

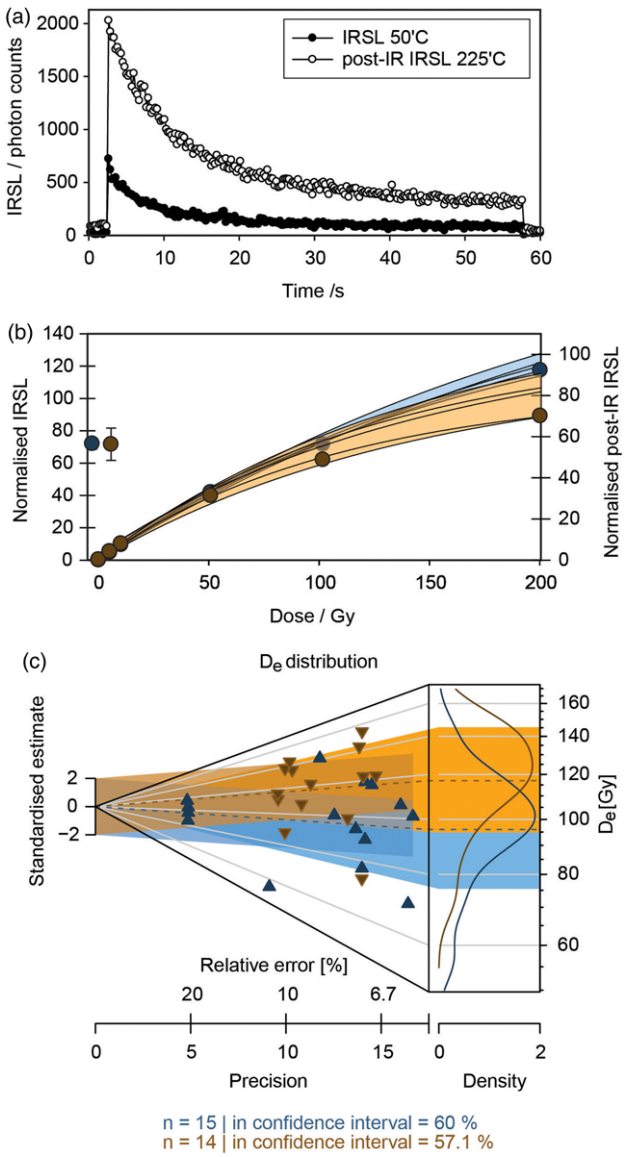

Fig. 4. (**a**) IRSL 50°C and post-IR IRSL 225°C decay curves for a single K-feldspar aliquot of SUTL2698; (**b**) IRSL 50°C and post-IR IRSL 225°C composite dose-response curves for SUTL2698; the composite responses are shown; (**c**) equivalent dose distributions for IRSL 50°C and post-IR IRSL 225°C.

Luminescence ages were calculated using standard microdosimetric models, with uncertainties that combined measurement and fitting errors from the SAR analysis, all dose rate evaluation uncertainties, and allowance for the calibration uncertainties of the sources and reference materials. The post-IR IRSL 225°C age estimates are (SUTL2698) 76.1 ± 3.5 ka and (SUTL2699) 58.7 ± 2.6 ka (Table 3).

The OSL dates from the K5 terrace come from aeolian grainstones along the northern coast. Both of the dated deposits are preserved at modern sea level but are 30 km apart along the coast. These deposits are interpreted as two distinct aggradation events at 76.1 and 58.7 ka during marine isotope stage (MIS) 4. Both deposits are interpreted as belonging to the K5 terrace and are likely to record different depositional phases within a single terrace system.

Age of pre-uplift deposits

An additional aim of this study was to achieve a better understanding of the timing of deposition prior to the first major uplift of the Kyrenia Range. Dating of the pre-uplift deposits was previously achieved through a combination of foraminiferal biozonation (Baroz 1979; Hakyemez *et al.* 2000; A. Lord, cited in Harrison *et al.* 2008) and limited strontium isotopic dating (McCay *et al.* 2012).

Deposition prior to major uplift is represented by the Nicosia (Lefkoşa) and Athalassa (Gürpınar) Formations (Ducloz 1972; Baroz 1979). The Nicosia (Lefkoşa) Formation comprises interbedded chalks and marls, whereas the Athalassa (Gürpınar) Formation is dominated by neritic grainstone facies (Palamakumbura & Robertson 2016) (Table 1; Fig. 3f). Here we use the traditional classification of the Athalassa (Gürpınar) Formation by Ducloz (1972). Dating of these deposits has been achieved using a combination of foraminiferal biozonation, palaeomagnetism and strontium isotope dating. The Nicosia (Lefkoşa) and Athalassa (Gürpınar) Formations are exposed within the Mesaoria (Mesorya) Basin between the Kyrenia Range and the Troodos Massif (Fig. 2). During this work samples were collected from the northern part of the Mesaoria Basin, close to the Kyrenia Range (north of the Ovgos (Dar Dere) Fault).

Table 3. *Optically stimulated luminescence (OSL) data for the K5 terrace aeolianite near the northern coast*

Sample	Latitude, longitude	Dose rate (mGy a^{-1})	Stimulation type	Equivalent dose (D_e) (Gy)	OSL age (ka)	Height (m AMSL)
KY14-01 (SUTL2698)	35°20.040'N, 33°29.239'E	1.47 ± 0.09	IRSL	98.8 ± 1.4		4
			Post-IR IRSL	**11.2 ± 2.6**	76.1 ± 3.5	
KY14-02 (SUTL2699)	35°24.817'N, 33°48.716'E	1.76 ± 0.01	IRSL	64.1 ± 0.8		0
			Post-IR IRSL	**94.7 ± 2.1**	53.7 ± 2.6	

Equivalent doses used for calculating the final OSL dates are shown in bold.

Strontium ($^{87}Sr/^{86}Sr$) dating

Strontium isotope dating is based on comparing the $^{87}Sr/^{86}Sr$ ratio from a sample with $^{87}Sr/^{86}Sr$ ratios in global oceans through time, expressed as a reference curve (McArthur *et al.* 2001). Two types of sample were used for the present strontium analysis, oyster shells and bulk grainstone (Table 4). Oysters were used as they are abundant and relatively well preserved, in contrast to most other bivalves in the deposits. The samples were collected from the upper part of the Athalassa (Gürpınar) Formation (Table 4). The oyster shells appear to be well preserved and in life position within benthic foraminifera-rich grainstones. Preparation of the oyster shells for analysis was carried out using the method of Henderson *et al.* (1994), whereas the preparation of the bulk grainstone followed that of Bailey *et al.* (2000). The strontium analysis was carried out at SUERC, East Kilbride on a VG Sector 54-30 mass spectrometer in a dynamic multi-collection mode.

Based on point counting, the grainstones analysed for strontium dating comprise abundant benthic foraminifera (*c.* 54%), mostly Peneroplidae, together with planktic foraminifera (*c.* 12%), reworked echinoderms (*c.* 4%), calcareous red algae (*c.* 5%), bivalve shell fragments (*c.* 2%) and reworked siliciclastic material (*c.* 21%). The deposits include finely crystalline calcite spar cement that coats the grains and partially infills the pore space.

The oyster shells and the bulk grainstone yielded $^{87}Sr/^{86}Sr$ ratios ranging from 0.70872 to 0.70911, representing an inferred age range of 15.99–1.43 Ma (Middle Miocene to Middle Pleistocene).

The Miocene ages results are problematic because the Athalassa (Gürpınar) Formation is known to unconformably overlie the Late Eocene–Late Miocene Kythrea (Değirmenlik) Group, which in places terminates with gypsum that was precipitated during the Messinian salinity crisis (Baroz 1979; McCay *et al.* 2012). It seems, therefore, that the Miocene Sr isotopic ages have to be discounted. Possible reasons include diagenetic alteration of the oyster shells, reworking of older material or deposition in a semi-enclosed marine basin with abnormal strontium isotopic ratios. Reworking is unlikely because the oyster shells appear to be in life position within shallow-marine deposits. The samples dated as Miocene are from the central part of the Mesaoria (Mesarya) Basin, which was a narrow seaway between the Troodos and Kyrenia landmasses during Late Pliocene–Early Pleistocene time (McCallum & Robertson 1995*b*) in which salinity could have been anomalous. The most likely explanation for the age discrepancy is that the oyster shells were affected by diagenesis that altered the $^{87}Sr/^{86}Sr$ ratios. The one whole-rock sample that was dated (sample KY13-80) came from the Karpaz (Karpas) Peninsula in the far east of the Kyrenia Range (Fig. 2), an area with a more open-marine influence. The determined Early Pleistocene age is consistent with the expected age of the Athalassa (Gürpınar) Formation, compared with the known Pliocene age of the underlying Nicosia (Lefkoşa Formation), as discussed below. However, no reliance can be placed on a single age result.

Palaeomagnetic dating

Palaeomagnetic dating has previously been used to help constrain the age of Pliocene and Pleistocene shallow-marine sediments around the southern and eastern margins of the Troodos Massif (Kinnaird *et al.* 2011; Weber *et al.* 2011). A similar approach was adopted for the sedimentary rocks exposed within and adjacent to the Kyrenia Range during this study. Samples were collected using a portable petrol drill and oriented using a sun compass, according to standard field methods (Butler 1992). After conventional measurement and analysis, it had to be concluded that none of the samples from the relatively young ('Pleistocene') terrace deposits on either flank of the Kyrenia Range yielded viable palaeomagnetic results (Palamakumbura 2015). However, the pre-uplift sequence exposed on the outer southern flank of the range provided worthwhile palaeomagnetic data.

The successful palaeomagnetic analysis was carried out on shallow-marine grainstones of the Athalassa (Gürpınar) Formation. Ninety-five cores from 19 sites were collected from the Nicosia (Lefkoşa) Formation and the overlying Athalassa (Gürpınar) Formation. All of the samples were first studied utilizing alternating-field (AF) demagnetization techniques at the National Oceanography Centre, University of Southampton and were measured using a 2G Enterprise Superconducting Rock Magnetometer. This revealed that 50 of the cores had a sufficiently intense magnetic signal to warrant thermal demagnetization, which was carried out on sister samples using a 2G Enterprises DC Squid

Table 4. *Strontium isotope results, standard percentage error and age (Ma) based upon the LOWESS marine Sr-isotope curve produced by McArthur et al. (2001)*

Sample	Latitude, longitude	Material	$^{87}Sr/^{86}Sr$	% Standard error	Age range (Ma)
KYSR-01	35°13.089'N, 33°48.756'E	*Ostrea, gryphaea*	0.708768	0.0014	15.13 – 15.35
KYSR-02	35°13.089'N, 33°48.756'E	*Ostrea, gryphaea*	0.708926	0.0014	7.97 – 8.88
KYSR-03	35°13.089'N, 33°48.756'E	*Ostrea, gryphaea*	0.708987	0.0014	6.06 – 6.14
KYSR-04	35°13.089'N, 33°48.756'E	*Ostrea, gryphaea*	0.70872	0.0013	15.81 – 15.99
KYSR-05	35°13.089'N, 33°48.756'E	*Ostrea, gryphaea*	0.709005	0.0013	5.75 – 5.86
KYSR-06	35°13.089'N, 33°48.756'E	*Ostrea, gryphaea*	0.708983	0.0015	6.11 – 6.20
KY13-45	35°11.764'N, 33°07.668'E	Grainstone	0.70897	0.0015	6.40 – 6.56
KY13-50	35°12.014'N, 33°07.004'E	Grainstone	0.708829	0.0012	12.05 – 12.12.63
KY13-52	35°11.205'N, 33°05.423'E	Grainstone	0.708699	0.0015	16.24 – 16.46
KY13-80	35°22.724'N, 34°04.977'E	Grainstone	0.709106	0.0012	1.425 – 1.532
KY13-92	35°30.970'N, 34°18.781'E	Grainstone	0.708916	0.0012	8.72 – 9.33

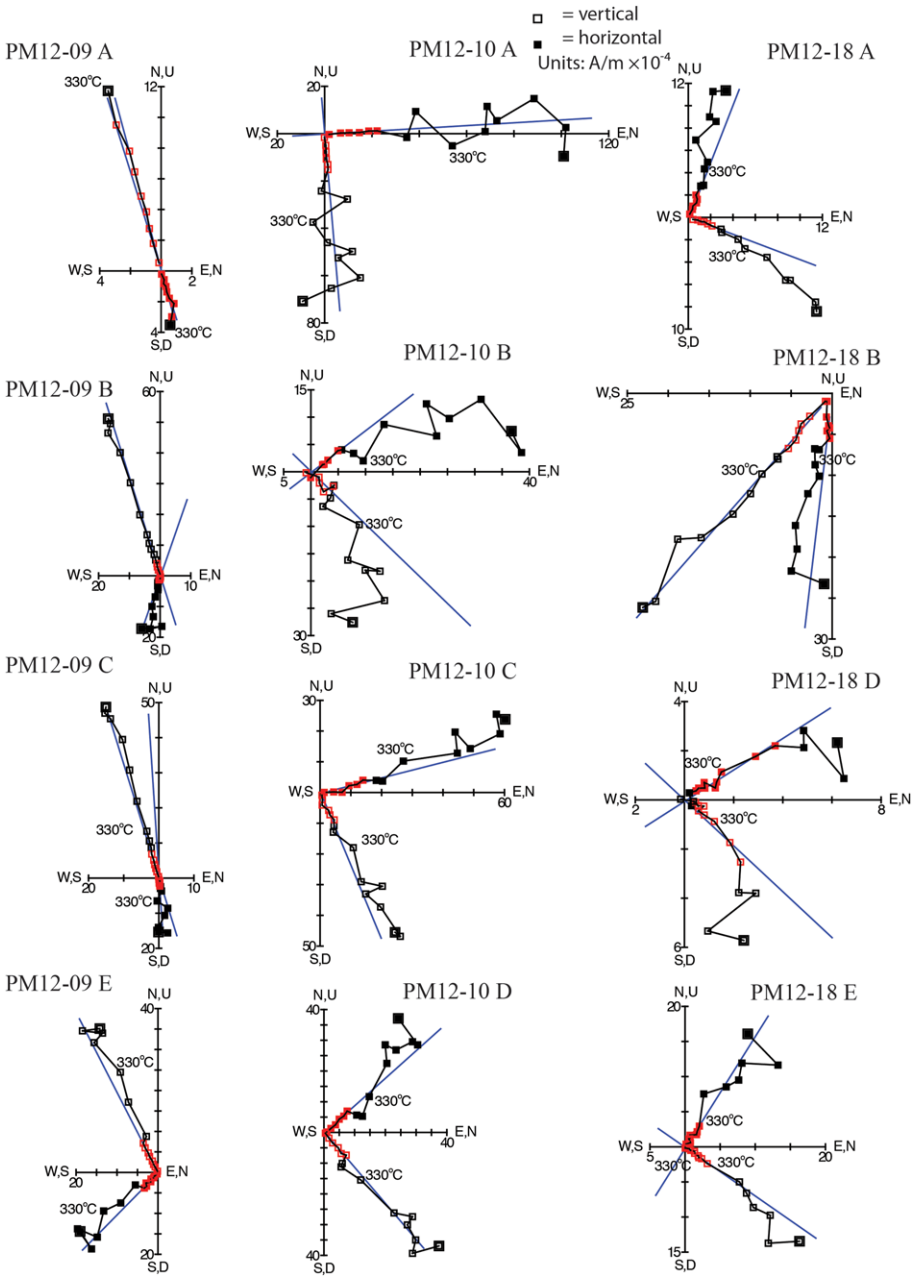

Fig. 5. Zijderveld plots from thermal demagnetization data that were used to calculate inclinations and declinations (Zijderveld 1967). The data were plotted using PuffinPlot (Lurcock & Wilson 2012).

Cryogenic Magnetometer at the University of Oxford. The thermal demagnetization steps used 50°C steps from 0 to 300°C, followed by 30°C steps, up to 590°C. Assessment of the quality of the data was mainly based upon inspection of the resulting Zeijderveld plots and from the intensity-decay curves (Zijderveld 1967). Each sample was ranked from A to C using the system developed by Richter *et al.* (1998), with A representing samples with a clear stable magnetic direction and C samples with either unstable directions or no magnetic signal. The A and B quality data were selected for principal component analysis (PCA).

When analysed using conventional methods (Butler 1992) the stepwise thermal demagnetization experiments revealed stable components of magnetization in 15 of the grainstone samples (Fig. 5 and Table 5). These samples were selected for magnetostratigraphic analysis. Figure 5 shows orthogonal projections of the thermal demagnetization data. The samples show a general reduction in magnetic signal intensity with increasing temperature. Removal of an unstable low-temperature signal (20–400°C) revealed a stable high-temperature direction of demagnetization between 400 and 590°C. This high-temperature style end-point direction was used to calculate the primary palaeomagnetic direction for each sample (Table 5).

Although the primary magnetization could be isolated in only 15 samples, it is clearly identified as having a dual polarity within the Athalassa (Gürpınar) Formation, with samples from the lower part of the sequence (sample PM12-08 A, B, D, E and PM12-10 A, B, C, D; Fig. 5 and Table 5) being of normal polarity (northward with positive inclinations) whereas the samples from the higher part of the sequence (PM12-09 A, B, C, D, E; Fig. 5 and Table 5) are of inverse polarity (southward and negative). The low α_{95} and high κ values for sites PM12-09 and PM12-10 (Table 5) are indicative of reasonably robust data. Site PM12-18 has relatively high α_{95} and low κ values indicating a less reliable dataset.

The large scatter of inclination values is possibly due to local sedimentary processes such as current orientation of grains (Kodama 2012). Sediment compaction was previously inferred to have affected measured inclination values in the Pliocene–Pleistocene sediments from the southern part of Cyprus (Kinnaird *et al.* 2011).

Despite the limitations of data quality, the palaeomagnetic results from the Athalassa (Gürpınar) Formation suggest that the deposition spanned a geomagnetic reversal. Reversed polarity grainstone deposits overlie normal polarity grainstones. The reversed polarity grainstones are interpreted as having been deposited before the

Table 5. *Results of thermal demagnetization of samples from the Athalassa (Gürpınar) Formation*

Sample	PCA declination	PCA inclination	Fisher declination	Fisher inclination	Fisher α_{95}	Fisher κ	Ranking of Richter *et al.* (1998)	Magnetic polarity
PM12-09A	166.97	−75.01	198.6	−70.7	15.8	35	A	Reversed
PM12-09B	191.17	−71.06					A	
PM12-09C	175.59	−73.25					A	
PM12-09E	229.41	−55.61					A	
PM12-10A	10.5	34.2	342.2	33.9	19	24.3	A	Normal
PM12-10B	331.2	25.4					B	
PM12-10C	350.4	28.4					A	
PM12-10D	331.5	34.6					A	
PM12-18A	48.6	13.8	50.6	38.5	71	2.7	B	Normal
PM12-18B	210.1	56.5					B	
PM12-18D	61	21.6					B	
PM12-18E	30.2	20.2					B	

Brunhes Chron, which marks the beginning of the Middle Pleistocene (Fig. 6). We have no constraints on the specific chrons with which these deposits could correlate, although an Early Pleistocene age is likely in view of the Pliocene age of the underlying Nicosia (Lefkoşa) Formation (see below).

Discussion

Timing of uplift

The viable results from the different dating techniques are shown in Figure 6 in relation to the Pliocene–Pleistocene stratigraphy of the Kyrenia Range. Mapping and sedimentological studies around the southern flank of the Kyrenia Range indicate that the entire intact Pliocene succession predates the oldest marine terrace deposits (K2), which occur at heights of up to 160 m AMSL (Palamakumbura 2015; Palamakumbura & Robertson 2016).

The chalks and marls of the Nicosia (Lefkoşa) Formation are rich in planktonic foraminifera, including *Globorotalia magaritae* and *Globorotalia acostaensis* (Baroz 1979; Hakyemez *et al.* 2000; A. Lord, pers. comm. 2015). The biota identified within the Nicosia (Lefkoşa) Formation can be interpreted as Early to Late Pliocene age based on up-to-date statigraphical correlations with oceanic deposits (Lourens *et al.* 2004; Wade *et al.* 2011). Several boreholes in the Greater Lefkoşa (Nicosia) area provide additional data on the age of the Nicosia (Lefkoşa) Formation. The planktonic foraminiferal assemblages are indicative of zones N19 to N20, of Pliocene age (A. Lord, cited by Harrison *et al.* 2008). The pre-uplift open-marine environment represented by the Nicosia (Lefkoşa) Formation is, therefore, inferred to have existed during the Pliocene. It should be noted that sediments of the Mesaoria (Mesorya) Group are not preserved along the northern flank of the Kyrenia Range although they may originally have been deposited there.

The Athalassa (Gürpınar) Formation conformably overlies the Nicosia (Lefkoşa) Formation within the northern part of the Mesaoria (Mesarya) Basin (Baroz 1979; this study). Similar planktonic foraminifera to those within the Nicosia (Lefkoşa) Formation have previously been reported from the Athalassa (Gürpınar) Formation in this area (Baroz 1979; Hakyemez *et al.* 2000). The Athalassa (Gürpınar) Formation is dominated by carbonate grainstones that accumulated in a shallow-marine (sub-littoral) environment (Baroz 1979; McCallum & Robertson 1995*b*; Harrison *et al.* 2004). Petrographic study of the grainstone deposits indicates that the formation includes large amounts of reworked shallow-water bioclastic material and also reworked planktonic foraminifera (Palamakumbura 2015). Reworking of planktonic foraminifera is suggested by (1) broken or abraded tests, (2) infilling of chambers with a different diagenetic cement from that of the matrix and (3) local presence of pre-Pliocene species. Some of the planktonic foraminifera that have previously been identified from the Athalassa (Gürpınar) Formation (Baroz 1979; Hakyemez *et al.* 2000) are, therefore, likely to have been reworked from the Nicosia (Lefkoşa) Formation. However, some planktonic foraminifera appear to be contemporaneous; these are preserved as intact tests, which enclose fine-grained micrite of similar composition to the sedimentary matrix. The shallow-marine deposits of the Athalassa (Gürpınar) Formation accumulated during a period of, first reversed polarity, then normal polarity, which is consistent with an Early Pleistocene age.

The U-series dating constrains the age of several littoral marine horizons related to the K4 terrace. When plotted on a eustatic sea-level curve, utilizing a widely used oxygen isotope stratigraphy (Siddall *et al.* 2006), the absolute age results correspond to two interglacial periods, ranging from MIS 7 to MIS 5 (Fig. 6). The >350 ka U-series date is believed to be analytically valid but is difficult to interpret, because the coral in this terrace deposit is fragmentary and reworked.

In addition, the OSL data constrain the age of the aeolian deposits associated with the K5 terrace (Fig. 6). Comparison with the isotopic curve shows that the aeolian environment coincided with the most recent glacial periods of the Late Pleistocene. The relative sequence of deposition, as recorded in the K4 and K5 terraces, can be also applied to the K1–K3 terraces, with the shallow-marine deposits representing interglacial stages and the non-marine aeolian deposit representing a glacial stage. Each of the K1–K3 terraces comprises a basal marine deposit overlain by non-marine deposits, which are interpreted as representing a marine transgression, followed by a marine regression. The transgressive and regressive sedimentary sequence of each terrace is interpreted as representing a Pleistocene interglacial to glacial cycle. Extrapolating this concept allows the K1–K5 terraces to be tentatively correlated with several glacial cycles during the Late Pleistocene (Fig. 6). Based on this approach, the age of the K1–K3 terraces is suggested to be *c.* 0.5–0.2 Ma.

Several other age-related results have a bearing on any overall age model for the Pliocene–Pleistocene deposits (Fig. 6). OSL dating of coastal aeolianites from the Karpaz (Karpas) Peninsula, making up the eastern prolongation of the Kyrenia Range, has given ages of 1.5–0.4 ka, from the base to the top of the deposit (Erginal *et al.* 2012). These OSL dates indicate aeolian deposition during the most recent glacial period, consistent with our OSL results (Fig. 6). In addition, the marine gastropod *Strombus bubonius* has been identified within marine deposits of the K4 terrace near the

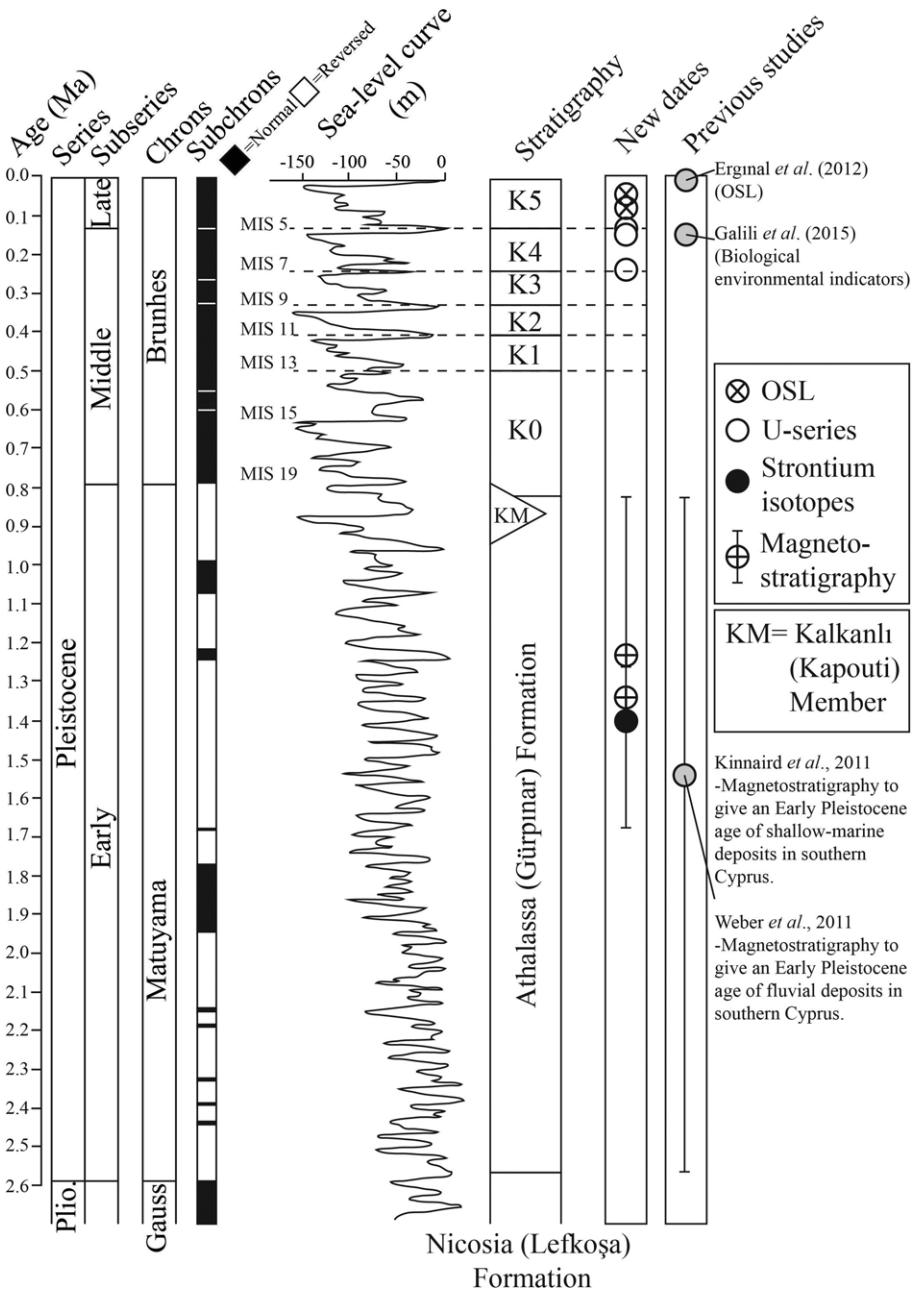

Fig. 6. Synthesis of new and previous dating carried out on Pleistocene deposits in northern Cyprus. The ages are from Ducloz (1972), Lord *et al.* (2000), Siddall *et al.* (2006) Kinnaird *et al.* (2011), Weber *et al.* (2011), Erginal *et al.* (2012) and Galili *et al.* (2015).

modern coastline (Ferranti *et al.* 2006; Galili *et al.* 2015). Warm-water conditions associated with MIS 5e are thought to have resulted in proliferation of this gastropod throughout the Mediterranean Sea at this time (Galili *et al.* 2015). This, in turn, suggests that the marine deposits containing *Strombus bubonius* are likely to have accumulated from 130 to 114 ka (MIS 5), which is broadly consistent with our U-series dating (Fig. 6).

Prior to the Early Pliocene, the Kyrenia Range and the Troodos Massif had been tectonically juxtaposed in their present positions, separated by the Mesaoria seaway (McCallum & Robertson 1990, 1995*b*). Neotectonic faulting is known to have been active along the Ovgos (Dar Dere) Fault during the Plio-Pleistocene, to the south of the Kyrenia Range (Harrison *et al.* 2004; McCay & Robertson 2012*b*). The question arises as to whether the emergent Troodos and Kyrenia areas were uplifted at similar or different times.

The deposits on the southern side of the Mesaoria (Mesarya) Basin can be stratigraphically correlated with similar deposits on the northern side of the Mesaoria (Mesarya) Basin (McCallum & Robertson 1990). The presence of non-marine, fluvial deposits (Apalos Formation) around the periphery of the Troodos Massif indicates that this area was above sea level by the Late Pliocene (McCallum & Robertson 1995*a*; Schirmer *et al.* 2010; Kinnaird *et al.* 2011; Weber *et al.* 2011). Throughout the Mesaoria (Mesarya) Basin, the mudstone and marl facies of the Nicosia (Lefkoşa) Formation pass transitionally upwards into bioclastic calcarenites of the Athalassa (Gürpınar) Formation. Close to the Kyrenia Range the succession continues upwards into lagoonal to non-marine, deltaic facies (Palamakumbura 2015; Palamakumbura & Robertson 2016).

Based on the microfossil evidence from the southern part of Cyprus (e.g. Pissouri Basin), Lord *et al.* (2000) inferred an Early to Late Pliocene age for the Nicosia (Lefkoşa) Formation. At that time, the Pliocene–Pleistocene boundary was placed at 1.8 Ma, thus placing the Athalassa (Gürpınar) Formation at least partially within the Pliocene. However, the more recently redefined boundary at 2.6 Ma (Cohen & Gibbard 2010) places most of the Athalassa (Gürpınar) Formation within the Pleistocene, throughout Cyprus. The available facies and dating evidence, therefore, suggests that the Troodos Massif and the Kyrenia Range were uplifted more or less simultaneously (Fig. 7).

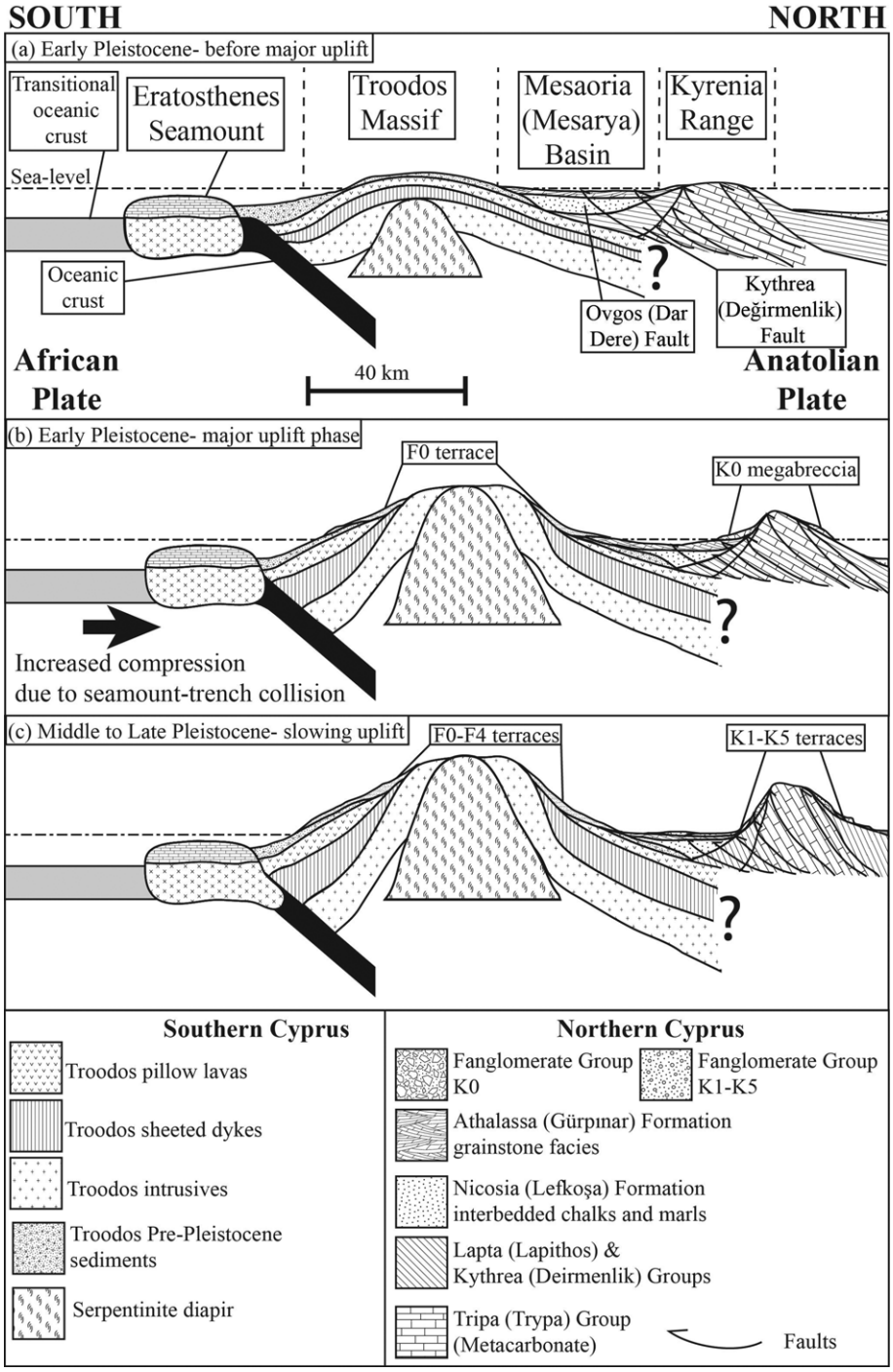

Fig. 7. Inferred tectonic diagram illustrating the preferred mechanism of Pleistocene uplift of the Kyrenia Range in the north of Cyprus.

Rates of uplift

Uplift rates can be estimated based on the inferred ages and the heights of successive terraces, field-based correlations, and both geomorphological and sea-level correlations (Table 6). In calculating uplift rates, the height and age of adjacent terraces were taken into account. The heights of the K4 and K5 terraces are those of the quantitatively dated deposits. The heights of the K1–K3 terraces are taken from the marine facies at the base of each terrace, which is observed to be the oldest part of the terrace. No marine facies are preserved within the K0 terrace that could be indicative of a base level; however, a height of 1000 m is used to represent the base level of the K0 terrace, which marks the start of uplift. The ages of the K4 and K5 terraces were determined by U-series disequilibria and OSL dating, whereas the K1–K3 ages were determined by correlations with the Pleistocene marine isotopic stages (see Table 6).

Using the age information, the amount of uplift that took place between the accumulation of the marine deposits of two successive terraces can be calculated. This allows the amount of uplift to be calculated between equivalent shallow-marine deposits within two different terraces. The K0–K2 terrace transition was chosen because the K0 and K1 terraces represent contemporaneous depositional environments (Palamakumbura 2015; Palamakumbura & Robertson 2016); therefore, the K0–K2 calculated uplift rate allows the K0 terrace deposits to be compared with the marine base of the K2 terrace. The calculated K3–K4 terrace uplift rate has a large uncertainty owing to the marine base of the K3 terrace being poorly preserved. Using the above method, the uplift rate between the K0–K2, K2–K3, K3–K4 terraces, within the K4 terrace and also between the K4–K5 terraces can all be calculated (Table 6).

The highest uplift rates were for the K0–K2 terrace, of >2 mm a^{-1} during the Middle Pleistocene. Uplift rates begin to

Table 6. *Summary of data used to calculate uplift rates: heights and ages from each of the terraces on the northern flanks of the Kyrenia Range; differences in heights and ages between terrace systems and the calculated uplift rates*

Terrace	Height (m)	Age (ka)	Age source
K0	1000	800	MIS 19(?)
K1	600	533	MIS 13
K2	140	424	MIS 11
K3	50	337	MIS 9
K4	40	243	U-series
K4	15	131	U-series
K5	1	60	OSL
Terraces	Height difference (m)	Age difference (ka)	Rate (mm a^{-1})
K0–K2	860	376	2.29
K2–K3	90	87	1.03
K3–K4	10	94	0.11(?)
K4–K4	25	112	0.22
K4–K5	14	71	0.21

fall for the K2–K3 terrace to *c.* 1 mm a^{-1} during the Middle Pleistocene. Finally, during the Late Pleistocene (K4 and K5 terraces) uplift rates were reduced to *c.* 0.2 mm a^{-1}. Two important implications are: first, the Kyrenia Range underwent rapid surface uplift during the Early to Middle Pleistocene and, second, the uplift was initially rapid and then slowed during the Middle to Late Pleistocene.

To put the calculated uplift rates in their regional context, it is interesting to draw comparisons with other areas of the easternmost Mediterranean that have also undergone major Pleistocene uplift (Table 7). First, areas to the east of Cyprus have undergone generally constant and slower uplift rates compared with the Kyrenia Range. The Lebanese coast, specifically, has apparently undergone constant, gradual uplift during the Pleistocene (Seyrek *et al.* 2008). Second, the calculated uplift rates for the Kyrenia Range and the Troodos Massif differ, the latter being generally faster. Nevertheless, the uplift rates of both the Troodos Massif and the Kyrenia Range appear to have been fastest during the Early Pleistocene, decreasing during the Middle and Late Pleistocene, as suggested by the age v. height AMSL model for both areas (i.e. for Troodos: Poole *et al.* 1990; for Kyrenia: this study).

Implication for processes of surface uplift

Cyprus and also southern Turkey (Schildgen *et al.* 2012) have undergone substantial Pleistocene uplift related to the convergence of the African and Eurasian plates. However, the scales of the uplifted areas vary regionally (Table 7), which needs to be taken into account in any tectonic interpretation. The narrow, uplifted Kyrenia Range is <6 km wide and >150 km long, whereas the domed uplift of the Troodos Massif is *c.* 50 km in circumference. The uplifted southern part of Anatolia and the Taurus Mountains is *c.* 150 km wide and >450 km long, whereas the roughly north–south-trending uplifted Amanos Mountains are *c.* 15 km across and *c.* 60 km long (Gomez *et al.* 2006). The uplifted Lebanese coastal area and is *c.* 200 km long and <50 km wide (Seyrek *et al.* 2008).

After a short-lived phase of thrusting, then emergence during Middle to Late Eocene time (Robertson *et al.* 2012), the Kyrenia Range became deeply submerged during the Oligocene to Mid-Miocene. This was followed by shelf-depth fine-grained deposition during the Late Miocene (McCay & Robertson 2012*a*), continuing after the Messinian salinity crisis during the Pliocene (Palamakumbura & Robertson 2016). In contrast, the Troodos Massif remained beneath a deep sea during Late Cretaceous to Oligocene time; initial uplift to shelf depths occurred during the Miocene, with localized emergence in the south prior to the Tortonian (Robertson 1977, 1990, 1998*a*). Following the Messinian salinity crisis, shelf-depth accumulation persisted around the periphery of the Troodos Massif until the Late Pliocene. Southern Anatolia was largely emergent by the Late Eocene following closure of a pre-existing Tethyan oceanic basin in the region (Clark & Robertson 2005). However, shallow-marine deposition persisted locally in southern Anatolia (e.g. in the Mut Basin) into the Pleistocene (Walsh-Kennedy *et al.* 2014). Southern Turkey was uplifted in stages over *c.* 23 myr, although uplift was fastest during the Pliocene–Pleistocene (Schildgen *et al.* 2012). In addition, the Lebanese coast and the Amanos Mountains regions were mainly uplifted during the Pliocene to Recent (Gomez *et al.* 2006; Seyrek *et al.* 2008).

Assuming the calculated uplift rates (Table 5) are broadly correct, the height differences between the Kyrenia Range and the Troodos Massif could simply reflect differences in uplift rates. However, assuming a similar uplift rate for the Kyrenia Range to that for the Troodos Massif, it is difficult to imagine the narrow Kyrenia Range ever reaching *c.* 2000 m AMSL, because it would have collapsed before reaching anything like this height. The lithologies of the Kyrenia Range are highly fractured and faulted related to successive Late Cretaceous, Mid-Eocene and Late Miocene–earliest Pliocene stages of deformation (Robertson & Kinnaird 2016). Such inherited rheological weaknesses would have favoured rapid disintegration of the spine of the Kyrenia Range during and soon after rapid uplift.

Even at its present height the oldest terrace (K0, equivalent to the Karka terrace; Ducloz 1972; Dreghorn 1978) is dominated by megabreccias with blocks up to tens of metres in size, which document just such a collapse process (Palamakumbura 2015; Palamakumbura & Robertson 2016). No such sediments are preserved around the more broadly uplifted Troodos Massif (Poole & Robertson 1990).

Taking account of the extrapolated age data (see Table 5) and other constraints (e.g. lithology; structure), the Kyrenia Range is estimated to have been uplifted during the Early Pleistocene at >2 mm a^{-1}, which is significantly faster than for adjacent areas of the easternmost Mediterranean region. The Troodos Massif appears to have been uplifted at a maximum rate of 2.4 mm a^{-1},

Table 7. *Uplift rates (mm a^{-1}) of the Kyrenia Range compared with several other uplifted regions of the easternmost Mediterranean*

Region	Pleistocene			Reference
	Early	Middle	Late	
Kyrenia Range	>1.2	1	0.2	This study
Troodos Massif	2.4	0.5	0.5	Poole *et al.* (1990)
SE Cyprus	–	–	1.8	Harrison *et al.* (2012)
Anatolian Plateau	0.72 – 0.74	0.6 – 0.7	0.6 – 0.7	Schildgen *et al.* (2012)
Lebanese coast	0.14	0.14	0.14	Gomez *et al.* (2006)
Amanos Mountains (SE Turkey)	0.25 – 0.4	0.25 – 0.4	0.25 – 0.4	Seyrek *et al.* (2008)

mostly during the Early Pleistocene (Poole *et al.* 1990). The massif was uplifted as a broad dome, supported by erosionally resistant ophiolitic diabase. In contrast to the Kyrenia Range, mass wasting (as opposed to normal fluvial deposition) is seen only locally; for example, around parts of the serpentinite core where the topography is unusually steep (e.g. Amiandos area; Poole & Robertson 1998).

Despite the differences in inferred maximum uplift rate and lithology between the Kyrenia Range and the Troodos Massif it appears that the timing and rates of uplift of the two areas are more similar to each other than to those of any of the adjacent areas discussed above (e.g. southern Turkey; Amanos Mountains, Lebanese coast). This, in turn, points to a single overall driving mechanism for the uplift of both the Troodos Massif and the Kyrenia Range. The uplift of the Troodos Massif has previously been explained by the collision of the Eratosthenes Seamount, a crustal edifice, with the Cyprus trench to the south of Cyprus (Robertson 1990, 1998*c*, 2000; Robertson & Grasso 1995; Kempler 1998; Mart *et al.* 1997). It has also been suggested that the domal Troodos uplift might relate to sepentinization of the underlying mantle wedge (Robertson 1990, 2000; Poole & Robertson 1991; see also Shelton 1993). The collision of the Eratosthenes Seamount could also have driven the uplift of the Kyrenia Range, assuming that this was kinematically coupled with the Troodos Massif, explaining the similarities in the timing and rates of uplift of the two areas (Fig. 7). The entire process occurred within a region of dominantly compressional tectonics (Le Pichon & Kreemer 2010; Seyrek *et al.* 2014), which was locally exaggerated by the collision of the Eratosthenes Seamount with the Cyprus active margin. This would also explain why the Kyrenia Range reaches its maximum height at a similar longitude to both the Eratosthenes Seamount and the Troodos Massif, and also why the Kyrenia Range submerges both to the east and the west away from the inferred north–south collision zone.

Several alternative driving mechanisms for the regional-scale uplift of the Troodos Massif and the Kyrenia Range can also be considered. One involves strike-slip or transpression during the Pliocene–Pleistocene tectonic escape of Anatolia towards the Aegean region (Harrison *et al.* 2004; Jaffey & Robertson 2005). Strike-slip has indeed been found to play an important role related to the Ovgos (Dar Dere) Fault, which essentially separates crust related to the Kyrenia Range from that related to the Troodos Massif (Harrison *et al.* 2004; McCay & Robertson 2012*b*). However, there is no structural evidence of transpression of Pliocene age either within the Kyrenia Range (Palamakumbura 2015) or from scarce published seismic reflection data (Aksu *et al.* 1992; Calon *et al.* 2005*a*). Another alternative involves crustal extension. Extensional tectonics have played an important role in the easternmost Mediterranean region (Glover & Robertson 2004). Offshore seismic data from the Cilicia and Latakia Basins adjacent to Cyprus indicate the presence of extensional structures within pre-Pliocene units based on offshore seismic data (e.g. Calon *et al.* 2005*b*). Onshore field studies in southern Turkey are also indicative of crustal extension, as noted around the periphery of the Gulf of Iskenderun (Boulton & Robertson 2008). In addition, the Hatay Graben is inferred to represent a transition from extension to transtension during the Miocene to Pleistocene, probably as a consequence of the regional westward tectonic escape of Anatolia (Boulton & Robertson 2008). Also, to the west of the Eratosthenes Seamount, crustal extension took place within the Polis Graben of western Cyprus, continuing into the Pleistocene (Payne & Robertson 1995). Such areas affected by Pleistocene extension are located well to the east or the west of the inferred roughly north–south Eratosthenes–Troodos–Kyrenia collision zone.

The Plio-Pleistocene uplift of the southern Anatolian plateau and the Taurus Mountains generally has recently been attributed to the break-off, tearing or delamination of the down-going African plate in the region (Faccenna *et al.* 2006; Cosentino *et al.* 2012; Schildgen *et al.* 2012). Such slab disruption might also have influenced the uplift of the Kyrenia Range. However, the Kyrenia Range is located 200 km south of the inferred location of the tear in the downgoing slab, whereas the Anatolian Plateau is located directly above this inferred feature (Schildgen *et al.* 2014).

The rapid uplift rates inferred during the Pleistocene uplift of the Kyrenia Range suggest that tectonic uplift was the dominant control on deposition during this time, modified by the effects of sea-level change and related climatic change. The uplift rates and preserved altitudes of the older and higher terraces are much greater than could be explained by eustatic sea-level change on its own. However, the inference that tectonic uplift slowed markedly during the Middle to Late Pleistocene means that eustatic sea-level change is likely to have played a relatively greater role in the formation of the younger and lower terraces.

Conclusions

(1) The uplift of the Kyrenia Range occurred within a regional-scale plate convergence zone in the Eastern Mediterranean region and can thus provide insights into fundamental crustal processes.

(2) Shallow-marine sediments, mostly open-marine marls that predated major uplift, are dated as Pliocene, using a combination of available microfossil dating and mostly existing Sr isotopic evidence.

(3) New palaeomagnetic evidence for overlying shallow-marine carbonate sediments indicates accumulation during reversed and normal polarity intervals, consistent with an Early Pleistocene age.

(4) U-series dating of aragonitic *Cladocora* coral from the youngest of four uplifted littoral marine terraces (K4 terrace) along the northern coast of Cyprus indicates deposition at >350, 243, 131 and 127 ka (equivalent to MIS 9, 7 and 5).

(5) OSL dating of aeolian grainstones overlying the youngest marine terrace (K5) indicates accumulation from 76 to 53 ka.

(6) Correlation of the available age data (new and existing) from the littoral-marine terrace deposits with the eustatic sea-level curve based on the oceanic oxygen isotope record indicates that the dated coral-bearing littoral deposits accumulated during eustatic sea-level highs, whereas the dated aeolianites formed during regressive periods.

(7) The well-established dates for the younger (K4 and K5) littoral terraces can be used to calculate rates of uplift of <0.2 mm a^{-1} during the Late Pleistocene.

(8) The older, topographically higher littoral terraces along the northern flank of the Kyrenia Range can be correlated with earlier major marine transgressions (MIS 13, 11 and 9), suggesting that the Kyrenia Range was uplifted at maximum rates of either 1.2 or >2 mm a^{-1} during early Pleistocene time.

(9) Comparison of the inferred uplift rates of the Kyrenia Range and the Troodos Massif with those for adjacent areas of the easternmost Mediterranean region suggests similar timings and rates of uplift of the two crustal units in Cyprus, which differ from those for southern Turkey and the Lebanese coast.

(10) The Pleistocene uplift of the Troodos Massif can be explained by the collision of the Eratosthenes Seamount with the Cyprus trench, and the near-simultaneous uplift of the Kyrenia Range directly to the north is likely to have a similar cause.

Acknowledgements and Funding

R.N.P. acknowledges the NERC CASE scholarship at the University of Edinburgh. Additional field and laboratory work was aided by the DARIUS Programme to A.H.F.R. and T.C.K. We are grateful for the additional financial support provided by the John Dixon Memorial Fund. R.N.P. also thanks É. Deady for help with the palaeomagnetic sampling. We thank M. Necdet for assistance with logistical aspects during the fieldwork. We also thank C. Mac Niocaill (University of Oxford) and C. Xuan (University of Southampton) for the use of palaeomagnetic laboratories and guidance with laboratory methods. A. Morris helped with interpretation of the palaeomagnetism data. We thank N. Odling for carrying out the XRD determination on the coral samples. A. Kelly kindly carried out the strontium dating at SUERC, East Kilbride. In addition, we thank R. Ellam and D. Sanderson for the use of the ICP-MS laboratory and the luminescence laboratories respectively, both at SUERC. The paper benefited from detailed comments from two anonymous referees.

Scientific editing by Erdin Bozkurt

References

Aksu, A.E., Calon, T.J., Piper, D.J.W., Turgut, S. & Izdar, E. 1992. Architecture of late orogenic Quaternary basins in northeastern Mediterranean Sea. *Tectonophysics*, **210**, 191–213.

Bailey, T.R., McArthur, J.M., Prince, H. & Thirlwall, M.F. 2000. Dissolution methods for strontium isotope stratigraphy: whole rock analysis. *Chemical Geology*, **167**, 313–319, http://doi.org/10.1016/S0009-2541(99)00235-1.

Barka, A. & Reilinger, R. 1997. Active tectonics of the Eastern Mediterranean region: deduced from GPS, neotectonic and seismicity data. *Annali di Geofisica*, **11**, 587–610.

Baroz, F. 1979. *Etude Géologique dans Le Pentadaktylos et La Mesaoria (Chypre Septentrionale).* Université de Nancy.

Bartol, J. & Govers, R. 2014. A single cause for uplift of the Central and Eastern Anatolian plateau? *Tectonophysics*, **637**, 116–136, http://doi.org/10.1016/j.tecto.2014.10.002.

Beets, C.J. & De Ruig, M.J. 1992. $^{87}Sr/^{86}Sr$ dating of coralline algal limestones and its implications for the tectono-stratigraphic evolution of the eastern Prebetic (Spain). *Sedimentary Geology*, **78**, 233–250, http://doi.org/10.1016/0037-0738(92)90022-J.

Berk Biryol, C., Beck, S.L., Zandt, G. & Özacar, A.A. 2011. Segmented African lithosphere beneath the Anatolian region inferred from teleseismic P-wave tomography. *Geophysical Journal International*, **184**, 1037–1057, http://doi.org/10.1111/j.1365-246X.2010.04910.x.

Boulton, S.J. & Robertson, A.H.F. 2008. The Neogene–Recent Hatay Graben, South Central Turkey: graben formation in a setting of oblique extension (transtension) related to post-collisional tectonic escape. *Geological Magazine*, **145**, 800–821, http://doi.org/10.1017/S0016756808005013.

Butler, R.F. 1992. *Paleomagnetism: Magnetic Domains to Geologic Terranes.* Blackwell, Boston, MA.

Buylaert, J.P., Murray, A.S., Thomsen, K.J. & Jain, M. 2009. Testing the potential of an elevated temperature IRSL signal from K-feldspar. *Radiation Measurements*, **44**, 560–565, http://doi.org/10.1016/j.radmeas.2009.02.007.

Calon, T.J., Aksu, A.E. & Hall, J. 2005*a*. The Oligocene–Recent evolution of the Mesaoria Basin (Cyprus) and its western marine extension, Eastern Mediterranean. *Marine Geology*, **221**, 95–120, http://doi.org/10.1016/j.margeo.2005.03.012.

Calon, T.J., Aksu, A.E. & Hall, J. 2005*b*. The Neogene evolution of the Outer Latakia Basin and its extension into the Eastern Mesaoria Basin (Cyprus), Eastern Mediterranean. *Marine Geology*, **221**, 61–94, http://doi.org/10.1016/j.margeo.2005.03.013.

Clark, M. & Robertson, A. 2005. Uppermost Cretaceous–Lower Tertiary Ülükişla Basin, south–central Turkey: Sedimentary evolution of part of a unified basin complex within an evolving Neotethyan suture zone. *Sedimentary Geology*, **173**, 15–51, http://doi.org/10.1016/j.sedgeo.2003.12.010.

Clark, M.K., House, M.A., Royden, L.H., Whipple, K.X., Burchfiel, B.C., Zhang, X. & Tang, W. 2005. Late Cenozoic uplift of southeastern Tibet. *Geology*, **33**, 525–528, http://doi.org/10.1130/G21265.1.

Cohen, K.M. & Gibbard, P.L. 2010. *Global Chronostratigraphical Correlation Table for the Last 2.7 Million Years*, Subcommission on Quaternary Stratigraphy (International Commission on Stratigraphy), Cambridge, UK.

Cosentino, D., Schildgen, T.F. *et al.* 2012. Late Miocene surface uplift of the southern margin of the Central Anatolian plateau, Central Taurides, Turkey. *Geological Society of America Bulletin*, **124**, 133–145, http://doi.org/10.1130/B30466.1.

De Vaumas, E. 1961. Further contributions to the geomorphology of Cyprus. *Annual Report of the Geological Survery Department, Cyprus (1960)*, 24–34.

Dilek, Y. & Sandvol, E. 2009. Seismic structure, crustal architecture and tectonic evolution of the Anatolian–African plate boundary and the Cenozoic orogenic belts in the Eastern Mediterranean region. *In*: Murphy, J.B., Keppie, J.D. & Hynes, A.J. (eds) *Ancient Orogens and Modern Analogues.* Geological Society, London, Special Publications, **327**, 127–160, http://doi.org/10.1144/SP327.8.

Dreghorn, W. 1978. *Landforms in the Girne Range Northern Cyprus.* Maden Tetkik ve Arama Enstitüsü, Ankara.

Ducloz, C. 1964. *Geological Map of the Central Kyrenia Range.* Geological Survey Department, Nicosia.

Ducloz, C. 1972. The geology of the Bellapais–Kythrea area of the Central Kyrenia Range. *Bulletin of the Cyprus Geological Survey Department*, **6**, 44–71.

Erginal, A.E., Kiyak, N.G. & Ertek, T.A. 2012. A new Late Holocene eolianite record from Altınkum beach, North Cyprus. *Turkish Journal of Earth Sciences*, **21**, 407–414, http://doi.org/10.3906/yer-0908-24.

Faccenna, C., Bellier, O., Martinod, J., Piromallo, C. & Regard, V. 2006. Slab detachment beneath eastern Anatolia: A possible cause for the formation of the North Anatolian fault. *Earth and Planetary Science Letters*, **242**, 85–97, http://doi.org/10.1016/j.epsl.2005.11.046.

Ferranti, L., Antonioli, F. *et al.* 2006. Markers of the last interglacial sea-level highstand along the coast of Italy: Tectonic implications. *Quaternary International*, **145–146**, 30–54, http://doi.org/10.1016/j.quaint.2005.07.009.

Galili, E., Şevketoğlu, M., Salamon, A., Zviely, D., Mienis, H., Rosen, B. & Moshkovitz, S. 2015. Late Quaternary beach deposits and archaeological relicts on the coasts of Cyprus, and the possible implications of sea-level changes and tectonics on the early populations. *In*: Harff, J., Bailey, G. & Lüth, F. (eds) *Geology and Archaeology: Submerged Landscapes of the Continental Shelf.* Geological Society, London, Special Publications, **411**, 179–218, http://doi.org/10.1144/SP411.10.

Gass, I.G. 1960. *The Geology and Mineral Resources of the Dhali Area.* Memoirs of the Cyprus Geological Survey Department, **4**, 116.

Glover, C.P. & Robertson, A.H.F. 2004. Role of regional extension and uplift in the Plio-Pleistocene evolution of the Aksu Basin, SW Turkey. *Journal of the Geological Society, London*, **155**, 365–387, http://doi.org/10.1144/gsjgs.155.2.0365.

Gomez, F., Khawlie, M., Tabet, C., Nasser Darkal, A., Khair, K. & Barazangi, M. 2006. Late Cenozoic uplift along the northern Dead Sea transform in Lebanon and Syria. *Earth and Planetary Science Letters*, **241**, 913–931, http://doi.org/10.1016/j.epsl.2005.10.029.

Gregory-Wodzicki, K.M. 2000. Uplift history of the Central and Northern Andes: a review. *Geological Society of America Bulletin*, **112**, 1091–1105, http://doi.org/10.1130/0016-7606(2000)112<1091:uhotca>2.0.co;2.

Hakyemez, Y., Turhan, N., Sönmez, I. & Sümengen, M. 2000. *Kuzey Kibris Türk Cumhuriyeti' Nin Jeolojisi (Geology of the Turkish Republic of Northern Cyprus)*, report of MTA (Maden Tektik ve Arama), Genel Mudurlugu Jeoloji Etutleri Diaresi, Ankara.

Harrison, B.R., Newell, W. *et al.* 2008. *Bedrock Geologic Map of the Greater Lefkosia Area, Cyprus.* [Accompanying pamphlet], US Geological Survey, Reston, VA.

Harrison, R.W., Newell, W.L. *et al.* 2004. Tectonic framework and Late Cenozoic tectonic history of the northern part of Cyprus: implications for earthquake hazards and regional tectonics. *Journal of Asian Earth Sciences*, **23**, 191–210, http://doi.org/10.1016/S1367-9120(03)00095-6.

Harrison, R.W., Tsiolakis, E., Stone, B.D., Lord, A., McGeehin, J.P., Mahan, S.A. & Chirico, P. 2012. Late Pleistocene and Holocene uplift history of Cyprus: implications for active tectonics along the southern margin of the Anatolian microplate. *In*: Robertson, A.H.F., Parlak, O. & Ünlügenç, U.C. (eds) *Geological Development of Anatolia and the Easternmost Mediterranean Region.* Geological Society, London, Special Publications, 561–584, http://doi.org/10.1144/SP372.3.

Henderson, G.M., Martel, D.J., O'Nions, R.K. & Shackleton, N.J. 1994. Evolution of seawater $^{87}Sr/^{86}Sr$ over the last 400 ka: the absence of glacial/interglacial cycles. *Earth and Planetary Science Letters*, **128**, 643–651.

Ivanovich, M. 1982. Uranium series disequilibria applications in geochronology. *In*: Ivanovich, M. & Harmon, R.S. (eds) *Uranium-Series Disequilibrium: Applications to Environmental Problems.* Oxford University Press, Oxford, 56–78.

Jaffey, N. & Robertson, A.H.F. 2001. New sedimentological and structural data from the Ecemiş Fault Zone, southern Turkey: implications for its timing and offset and the Cenozoic tectonic escape of Anatolia. *Journal of the Geological Society, London*, **158**, 367–378, http://doi.org/10.1144/jgs.158.2.367.

Jaffey, N. & Robertson, A.H.F. 2005. Non-marine sedimentation associated with Oligocene–Recent exhumation and uplift of the Central Taurus Mountains, S Turkey. *Sedimentary Geology*, **173**, 53–89, http://doi.org/10.1016/j.sedgeo.2003.11.025.

Kempler, D. 1998. Eratosthenes seamount: the possible spearhead of incipient continental collision in the Eastern Mediterreanean. *In*: Robertson, A.H.F., Emeis, K., Richter, C. & Camerlenghi, A. (eds) *Proceedings of the Ocean Drilling Program, Scientific Results,* **160**. Ocean Drilling Program, College Station, TX, 709–721.

Kempler, D. & Garfunkel, Z. 1994. Structures and kinematics in the northeastern Mediterranean: A study of an irregular plate boundary. *Tectonophysics*, **234**, 19–32, http://doi.org/10.1016/0040-1951(94)90202-X.

Kinnaird, T. & Robertson, A. 2013. Tectonic and sedimentary response to subduction and incipient continental collision in southern Cyprus, easternmost Mediterranean region. *In*: Robertson, A.H.F., Osman, P. & Ünlügenç, U.C. (eds) *Geological Development of Anatolia and the Easternmost Mediterranean Region.* Geological Society, London, Special Publications, **372**, 585–613, http://doi.org/10.1144/SP372.10.

Kinnaird, T.C., Robertson, A.H.F. & Morris, A. 2011. Timing of uplift of the Troodos Massif (Cyprus) constrained by sedimentary and magnetic polarity evidence. *Journal of the Geological Society, London*, **168**, 457–470, http://doi.org/10.1144/0016-76492009-150.

Kinnaird, T.C., Sanderson, D.C.W. & Bigelow, G.F. 2015. Feldspar SARA IRSL dating of very low dose rate aeolian sediments from Sandwick South, Unst, Shetland. *Quaternary Geochronology*, **30**, 1–7, http://doi.org/10.1016/j.quageo.2015.02.019.

Knup, P.E. 1965. *Geological Map of the Central Kyrenia Range.* Geological Survey Department, Nicosia.

Kodama, K.P. 2012. *Paleomagnetism of Sedimentary Rocks: Process and Interpretation.* Wiley, Chichester.

Le Pichon, X. & Kreemer, C. 2010. The Miocene-to-Present kinematic evolution of the Eastern Mediterranean and Middle East and its implications for dynamics. *Annual Review of Earth and Planetary Sciences*, **38**, 323–351, http://doi.org/10.1146/annurev-earth-040809-152419.

Lord, A.R., Panayides, E.U. & Xenophontos, C. 2000. A biochronostratigraphical framework for the Late Cretaceous–Recent circum-Troodos sedimentary sequence, Cyprus. *In*: Panayides, I., Xenophontos, C. & Malpas, J. (eds) *Proceedings of the Third International Conference on the Geology of the Eastern Mediterranean.* Geological Survey Department, Nicosia, 289–297.

Lourens, L.J., Hilgen, F.J., Shackleton, N.J., Laskar, J. & Wilson, D. 2004. The Neogene Period. *In*: Gradstein, F.M., Ogg, J.G. & Smith, A.G. (eds) *Geological Time Scale 2004.* Cambridge University Press, Cambridge, 409–440.

Lurcock, P.C. & Wilson, G.S. 2012. PuffinPlot: A versatile, user-friendly program for paleomagnetic analysis. *Geochemistry, Geophysics, Geosystems*, **13**, 1–6, http://doi.org/10.1029/2012GC004098.

Main, C.E., Robertson, A.H.F. & Palamakumbura, R.N. 2016. Pleistocene geomorphological and sedimentary development of the Akaki River catchment (northeastern Troodos Massif) in relation to tectonic uplift v. climatic change. *International Journal of Earth Sciences*, **105**, 463–485, http://doi.org/10.1007/s00531-015-1251-6.

Mart, Y., Robertson, A.H.F. & Woodside, J.M. 1997. Cretaceous tectonic setting of Eratosthenes Seamount in the eastern Mediterranean Neotethys: initial results of ODP Leg 160. *Comptes Rendus de l'Académie des Sciences, Série 2*, **324**, 127–134.

McArthur, J.M., Howarth, R.J. & Bailey, T.R. 2001. Strontium isotope stratigraphy: LOWESS version 3: best fit to the marine Sr-isotope curve for 0–509 Ma and accompanying look-up table for deriving numerical age. *Journal of Geology*, **109**, 155–170, http://doi.org/10.1086/319243.

McCallum, J.E. & Robertson, A.H.F. 1990. Pulsed uplift of the Troodos Massif—evidence from the Plio-Pleistocene Mesaoria basin. *In*: Malpas, J., Moores, E. M., Panayiotou, A. & Xenophontos, C. (eds) *Troodos '87, Ophiolite and Oceanic Lithosphere.* Geological Survey Department, Nicosia, 217–230.

McCallum, J.E. & Robertson, A.H.F. 1995*a*. Sedimentology of two fan–delta systems in the Pliocene–Pleistocene of the Mesaoria Basin, Cyprus. *Sedimentary Geology*, **98**, 215–244.

McCallum, J.E. & Robertson, A.H.F. 1995*b*. Late Pliocene–early Pleistocene Athalassa Formation, north central Cyprus: carbonate sand bodies in a shallow seaway between two emerging landmasses. *Terra Nova*, **7**, 265–277.

McCay, G.A. 2010. *Tectonic–sedimentary evolution of the Girne (Kyrenia) Range and the Mesarya (Mesaoria) Basin, North Cyprus*. *PhD thesis*, University of Edinburgh.

McCay, G.A. & Robertson, A.H.F. 2012*a*. Late Eocene–Neogene sedimentary geology of the Girne (Kyrenia) Range, northern Cyprus: A case history of sedimentation related to progressive and diachronous continental collision. *Sedimentary Geology*, **265–266**, 30–55, http://doi.org/10.1016/j.sedgeo.2012.03.001.

McCay, G.A. & Robertson, A.H.F. 2012*b*. Upper Miocene–Pleistocene deformation of the Girne (Kyrenia) Range and Dar Dere (Ovgos) lineaments, northern Cyprus: role in collision and tectonic escape in the easternmost Mediterranean region. *In*: Robertson, A.H.F., Osman, P. & Ünlügenç, U.C. (eds) *Geological Development of Anatolia and the Easternmost Mediterranean Region.* Geological Society, London, Special Publications, **372**, 421–445, http://doi.org/10.1144/SP372.6.

McCay, G., Robertson, A.H.F., Kroon, D., Raffi, I., Ellam, R.M. & Necdet, M. 2012. Stratigraphy of Cretaceous to Lower Pliocene sediments in the northern part of Cyprus based on comparative $^{87}Sr/^{86}Sr$ isotopic, nannofossil and planktonic foraminiferal dating. *Geological Magazine*, **150**, 1–27, http://doi.org/10.1017/S0016756812000465.

McClusky, S., Reilinger, R., Mahmoud, S., Ben Sari, D. & Tealeb, A. 2003. GPS constraints on Africa (Nubia) and Arabia plate motions. *Geophysical Journal International*, **155**, 126–138, http://doi.org/10.1046/j.1365-246X.2003.02023.x.

Müller, D.W. 1993. Pliocene transgression in the western Mediterranean Sea: strontium isotopes from Cuevas del Almanzora (SE Spain). *Paleoceanography*, **8**, 127, http://doi.org/10.1029/92PA02795.

Palamakumbura, R.N. 2015. *Sedimentary response to the tectonic uplift of the Kyrenia Range, northern Cyprus, in its Eastern Mediterranean tectonic setting*. *PhD thesis*, University of Edinburgh.

Palamakumbura, R.N. & Robertson, A.H.F. 2016. Pleistocene terrace deposition related to tectonically controlled surface uplift: an example of the Kyrenia Range lineament in the northern part of Cyprus. *Sedimentary Geology*, **339**, 46–67, http://doi.org/10.1016/j.sedgeo.2016.03.022.

Palamakumbura, R.N., Robertson, A.H.F., Kinnaird, T.C. & Sanderson, D.C.W. 2016. Sedimentary development and correlation of Late Quaternary terraces in the Kyrenia Range, northern Cyprus, using a combination of sedimentology and optical luminescence data. *International Journal of Earth Sciences (Geologische Rundschau)*, **105**, 439–462, http://doi.org/10.1007/s00531-015-1173-3.

Payne, A.S. & Robertson, A.H.F. 1995. Neogene supra-subduction zone extension in the Polis graben system, west Cyprus. *Journal of the Geological Society, London*, **152**, 613–628, http://doi.org/10.1144/gsjgs.152.4.0613.

Poole, A.J. & Robertson, A.H.F. 1991. Quaternary uplift and sea-level change at an active plate boundary, Cyprus. *Journal of the Geological Society, London*, **148**, 909–921, http://doi.org/10.1144/gsjgs.148.5.0909.

Poole, A. & Robertson, A.H.F. 1998. Pleistocene fanglomerate deposition related to uplift of the Troodos Ophiolite, Cyprus. *In*: Robertson, A.H.F., Emeis, K.-C. & Camerlenghi, A. (eds) *Proceedings of the Ocean Drilling Program, Scientific Results,* **160**. Ocean Drilling Program, College Station, TX, 545–566.

Poole, A.J. & Robertson, A.H.F. 2000. Quaternary marine terrace and aeolinites in coastal south and west Cyprus: implications for regional uplift and sea-level change. *In*: Panayides, I., Xenophontos, C. & Malpas, J. (eds) *Proceedings of the Third International Conference on the Geology of the Eastern Mediterranean.* Geological Survey Department, Nicosia, 105–123.

Poole, A.J., Shimmield, G.B. & Robertson, A.H.F. 1990. Late Quaternary uplift of the Troodos ophiolite, Cyprus: Uranium-series dating of Pleistocene coral. *Geology*, **18**, 894–897.

Rhodes, E.J. 2011. Optically stimulated luminescence dating of sediments over the past 200,000 years. *Annual Review of Earth and Planetary Sciences*, **39**, 461–488, http://doi.org/10.1146/annurev-earth-040610-133425.

Richter, C., Roberts, A.P., Stoner, J.S., Benning, L.D. & Chi, C.T. 1998. Magnetostratigraphy of Pliocene–Pleistocene sediments from the eastern Mediterranean Sea. *In*: Robertson, A.H.F., Emeis, K. & Camerlenghi, A. (eds) *Proceedings of the Ocean Drilling Program, Scientific Results*, **160**. Ocean Drilling Program, College Station, TX, 61–73.

Roberts, G.P., Houghton, S.L. *et al.* 2009. Localization of Quaternary slip rates in an active rift in 105 years: An example from central Greece constrained by ^{234}U–^{230}Th coral dates from uplifted paleoshorelines. *Journal of Geophysical Research: Solid Earth*, **114**, 1978–2012, http://doi.org/10.1029/2008JB005818.

Robertson, A.H.F. 1977. Tertiary uplift history of the Troodos massif, Cyprus. *Geological Society of America Bulletin*, **12**, 1763–1772, http://doi.org/10.1130/0016-7606(1977)88<1763:TUHOTT>2.0.CO;2.

Robertson, A.H.F. 1990. Tectonic evolution of Cyprus. *In*: Malpas, J., Moores, E.M., Pamayiotou, A. & Xenophontos, C. (eds) *Ophiolites: Oceanic Crustal Analogues. Proceedings of the Symposium 'Troodos 1987'.* Geological Survey Department, Nicosia, 235–252.

Robertson, A.H.F. 1998*a*. Late Miocene paleoenvironments and tectonic setting of the southern margin of Cyprus and the Eratosthenes Seamount. *In*: Robertson, A.H.F., Emeis, K.-C., Richter, C. & Camerlengthi, A. (eds) *Proceedings of the Ocean Drilling Program Scientific Results.* **160**. Ocean Drilling Program, College Station, TX, 453–463.

Robertson, A.H.F. 1998*b*. Tectonic significance of the Eratosthenes Seamount: a continental fragment in the process of collision with a subduction zone in the eastern Mediterranean (Ocean Drilling Program Leg 160). *Tectonophysics*, **298**, 63–82, http://doi.org/10.1016/S0040-1951(98)00178-4.

Robertson, A.H.F. 1998*c*. Mesozoic–Tertiary tectonic evolution of the easternmost Mediterranean area: integration of marine and land evidence. *In*: Robertson, A.H.F., Emeis, K.-C., Richter, C. & Camerlenghi, A. (eds) *Proceedings of the Ocean Drilling Program, Scientific Results*, **160**. Ocean Drilling Program, College Station, TX, 723–782.

Robertson, A.H.F. 2000. Mesozoic–Tertiary tectonic–sedimentary evolution of a South Tethyan oceanic basin and its margins in Southern Turkey. *In*: Robertson, A.H.F. & Mountrakis, D. (eds) *Tectonic Development of the Eastern Mediterranean Region.* Geological Society, London, Special Publications, **173**, 97–138, http://doi.org/10.1144/GSL.SP.2000.173.01.05.

Robertson, A.H.F. & Grasso, M. 1995. Overview of the Late Tertiary-Recent tectonic and palaeo-environmental development of the Mediterranean region. *Terra Nova*, **7**, 114–127, http://doi.org/10.1111/j.1365-3121.1995.tb00680.x.

Robertson, A.H.F. & Kinnaird, T.C. 2016. Structural development of the central Kyrenia Range (north Cyprus) in its regional setting in the eastern Mediterranean region. *International Journal of Earth Sciences*, **105**, 417–437, http://doi.org/10.1007/s00531-015-1215-x.

Robertson, A.H.F. & Woodcock, N.H. 1986. The role of the Kyrenia Range Lineament, Cyprus, in the geological evolution of the Eastern Mediterranean area. *Philosophical Transactions of the Royal Society of London, Series A*, **317**, 141–177, http://doi.org/10.1098/rsta.1986.0030.

Robertson, A.H.F. & Xenophontos, C. 1993. Development of concepts concerning the Troodos ophiolite and adjacent units in Cyprus. *In*: Prichard, H.M., Alabaster, T., Harris, N.B. & Neary, C.R. (eds) *Magmatic Processes and Plate Tectonics.* Geological Society, London, Special Publications, **76**, 85–120, http://doi.org/10.1144/GSL.SP.1993.076.01.05.

Robertson, A.H.F., Parlak, O. & Ustaömer, T. 2012. Overview of the Palaeozoic–Neogene evolution of Neotethys in the Eastern Mediterranean region (southern Turkey, Cyprus, Syria). *Petroleum Geoscience*, **18**, 381–404, http://dx.doi.org/10.1144/petgeo2011-091.

Schattner, U. 2010. What triggered the early-to-mid Pleistocene tectonic transition across the entire eastern Mediterranean? *Earth and Planetary Science Letters*, **289**, 539–548, http://doi.org/10.1016/j.epsl.2009.11.048.

Schildgen, T.F., Cosentino, D. *et al.* 2012. Multi-phased uplift of the southern margin of the Central Anatolian plateau, Turkey: A record of tectonic and

upper mantle processes. *Earth and Planetary Science Letters*, **317–318**, 85–95, http://doi.org/10.1016/j.epsl.2011.12.003.

Schildgen, T.F., Yildirim, C., Cosentino, D. & Strecker, M.R. 2014. Linking slab break-off, Hellenic trench retreat, and uplift of the Central and Eastern Anatolian plateaus. *Earth-Science Reviews*, **128**, 147–168, http://doi.org/10.1016/j.earscirev.2013.11.006.

Schirmer, W., Weber, J. *et al.* 2010. Fluvial stacking due to plate collision and uplift during the Early Pleistocene in Cyprus. *Central European Journal of Geosciences*, **2**, 514–523, http://doi.org/10.2478/v10085-010-0023-6.

Seyrek, A., Demir, T. *et al.* 2008. Late Cenozoic uplift of the Amanos Mountains and incision of the Middle Ceyhan river gorge, southern Turkey; Ar–Ar dating of the Düziçi basalt. *Geomorphology*, **97**, 321–355, http://doi.org/10.1016/j.geomorph.2007.08.014.

Seyrek, A., Demir, T., Westaway, R., Guillou, H., Scaillet, S., White, T.S. & Bridgland, D.R. 2014. The kinematics of central–southern Turkey and northwest Syria revisited. *Tectonophysics*, **618**, 35–66, http://doi.org/10.1016/j.tecto.2014.01.008.

Shelton, A.W. 1993. Troodos revisited: the Mount Olympus gravity anomaly. *In*: Prichard, H., Alabaster, T., Harris, N.B. & Neary, C. (eds) *Magmatic Processes and Plate Tectonics.* Geological Society, London, Special Publications, 197–212, http://doi.org/10.1144/GSL.SP.1993.076.01.09.

Siddall, M., Chappell, J. & Potter, E. 2006. Eustatic sea level during past interglacials. *Developments in Quaternary Sciences*, **7**, 75–92.

Taylforth, J.E., McCay, G.A., Ellam, R., Raffi, I., Kroon, D. & Robertson, A.H.F. 2014. Middle Miocene (Langhian) sapropel formation in the easternmost Mediterranean deep-water basin: Evidence from northern Cyprus. *Marine and Petroleum Geology*, **57**, 521–536, http://doi.org/10.1016/j.marpetgeo.2014.04.015.

Thomsen, K.J., Murray, A.S. & Jain, M. 2011. Stability of IRSL signals from sedimentary K-feldspar samples. *Geochronometria*, **38**, 1–13, http://doi.org/10.2478/s13386-011-0003-z.

Turner, J.A., Leeder, M.R., Andrews, J.E., Rowe, P.J., Van Calsteren, P. & Thomas, L. 2010. Testing rival tectonic uplift models for the Lechaion Gulf in the Gulf of Corinth rift. *Journal of the Geological Society, London*, **167**, 1237–1250, http://doi.org/10.1144/0016-76492010-035.

Van Calsteren, P. & Thomas, L. 2006. Uranium-series dating applications in natural environmental science. *Earth-Science Reviews*, **75**, 155–175, http://doi.org/10.1016/j.earscirev.2005.09.001.

Van Calsteren, P. & Thomas, L. 2012. Quantitation of protactinium, ^{231}Pa in abyssal carbonate. *Journal of Analytical Atomic Spectrometry*, **27**, 952, http://doi.org/10.1039/c2ja30026e.

Wade, B.S., Pearson, P.N., Berggren, W.A. & Pälike, H. 2011. Review and revision of Cenozoic tropical planktonic foraminiferal biostratigraphy and calibration to the geomagnetic polarity and astronomical time scale. *Earth-Science Reviews*, **104**, 111–142, http://doi.org/10.1016/j.earscirev.2010.09.003.

Walsh-Kennedy, S., Aksu, A.E., Hall, J., Hiscott, R.N., Yaltirak, C. & Çifçi, G. 2014. Source to sink: The development of the latest Messinian to Pliocene–Quaternary Cilicia and Adana Basins and their linkages with the onland Mut Basin, eastern Mediterranean. *Tectonophysics*, **622**, 1–21, http://doi.org/10.1016/j.tecto.2014.01.019.

Weber, J., Schirmer, W., Heller, F. & Bachtadse, V. 2011. Magnetostratigraphy of the Apalós Formation (early Pleistocene): Evidence for pulsed uplift of Cyprus. *Geochemistry, Geophysics, Geosystems*, **12**, http://doi.org/10.1029/2010GC003193.

Weiler, Y. 1970. Mode of occurrence of pelites in the Kythrea Flysch basin (Cyprus). *Journal of Sedimentary Research*, **40**, 1255–1261.

Yetis, C., Kelling, G., Gökçen, S.L. & Baroz, F. 1995. A revised stratigraphic framework for Later Cenozoic sequences in the northeastern Mediterranean region. *International Journal of Earth Sciences*, **84**, 794–812.

Zijderveld, J.D.A. 1967. AC demagnetization of rocks: analysis of results. *In*: Collinson, D.W., Creer, K.M. & Runcorn, S.K. (eds) *Methods in Paleomagnetism 3.* Elsevier, Amsterdam, 254–286.